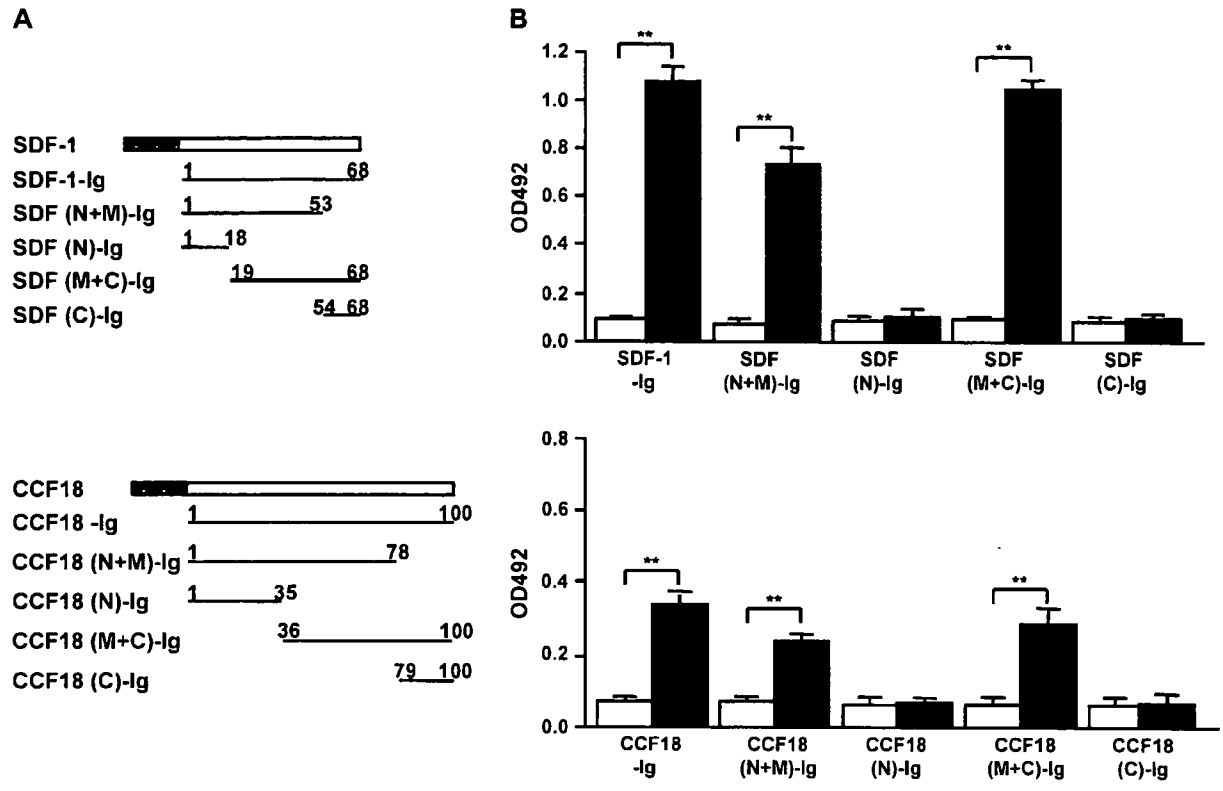

Figure 3. Determination of adiponectin-binding sites on chemokines. (A) Scheme of deleted stromal-derived factor–1 (SDF-1)– or CCF18-immunoglobulin (Ig) fusion proteins. The cDNA fragments of SDF-1 and CCF18 were amplified by polymerase chain reaction with primers as described in Materials and Methods, and cloned into the Ig/pEFBOSX vector. Amino acid numbers of mature proteins are shown. (B) Plasmids for producing the indicated Ig fusion proteins were transfected to 293T cells with calcium phosphate precipitation methods. After 3 days of cultures, each supernatant was collected and subjected to Western blots probed with anti-human Ig antibody. Ten micrograms per milliliter of BSA (open columns) or adiponectin (closed columns) was fixed on a microtiter tray at 4°C overnight. After blocking, supernatants containing each deleted SDF-1-Ig or CCF18-Ig were incubated at room temperature for 2 hours. The bound Ig-fusion proteins were detected with enzyme-linked immunosorbent assay using biotinylated anti-human Ig and avidin-biotin-alkaline phosophatase complex. Data are shown as mean ± SD of OD_{492} in tripricated samples. Statistically differences from control values are shown with two asterisks ($p < 0.01$). Similar results were obtained in three independent experiments.

recognizing CXCR4 inhibited the binding significantly. We next examined the chemotaxis of Jurkat cells by recombinant SDF-1. SDF-1 induced the migration activity and >40% of the cells moved to lower chambers within 30 minutes (Fig. 5B). While the migration was strongly abrogated by an anti-CXCR4 antibody, 10 to 20 μg/mL adiponectin showed little or no inhibitory or enhancing effects. Moreover, the Ca influx induced by recombinant SDF-1 was not affected by the addition of adiponectin (Fig. 5C). In the case of MCP-1, adiponectin failed to affect MCP-1–induced migration activity in THP-1 cells (data not shown). Therefore, adiponectin dose not influence chemokine–receptor interactions.

Adiponectin and heparan-sulfate proteoglycans influence each other on the binding to chemokines

Chemokines have positively charged domains, which are important to bind with heparan-sulfate proteoglycans (HSPG). The heparin-binding capacity involves in their localization and is required for their full-function in vivo [21]. We tested whether adiponectin influences the heparin-binding capacity of SDF-1 and MCP-1. Heparin Sephadex could precipitate recombinant SDF-1 and MCP-1, which were detectable with Western blot, and the binding was completely blocked by the addition of heparin (Fig. 6). When gAdiponectin was added to the mixture, SDF-1 and MCP-1 in the precipitates were decreased in a gAdiponectin dose-dependent manner (Fig. 6). Therefore, adiponectin reduces the binding capacity of chemokines to heparin.

The influence of heparin on the interaction between adiponectin and SDF-1 was evaluated using two experimental models, ELISA, and immunoprecipitation assays. When the binding of SDF-1–Ig and CCF18-Ig to adiponectin in the presence of heparin was evaluated with ELISA, their binding was completely inhibited by heparin (Fig. 7A). However, another adiponectin-binding protein, cystatin-C, recognized adiponectin even in the presence of heparin. Glutathione Sephadex was treated with gAdiponectin-GST fusion protein, and then the binding capacity of adiponectin-bearing Sephadex to recombinant SDF-1 in the presence of heparin was examined. The precipitate without heparin clearly contained SDF-1, but SDF-1 was

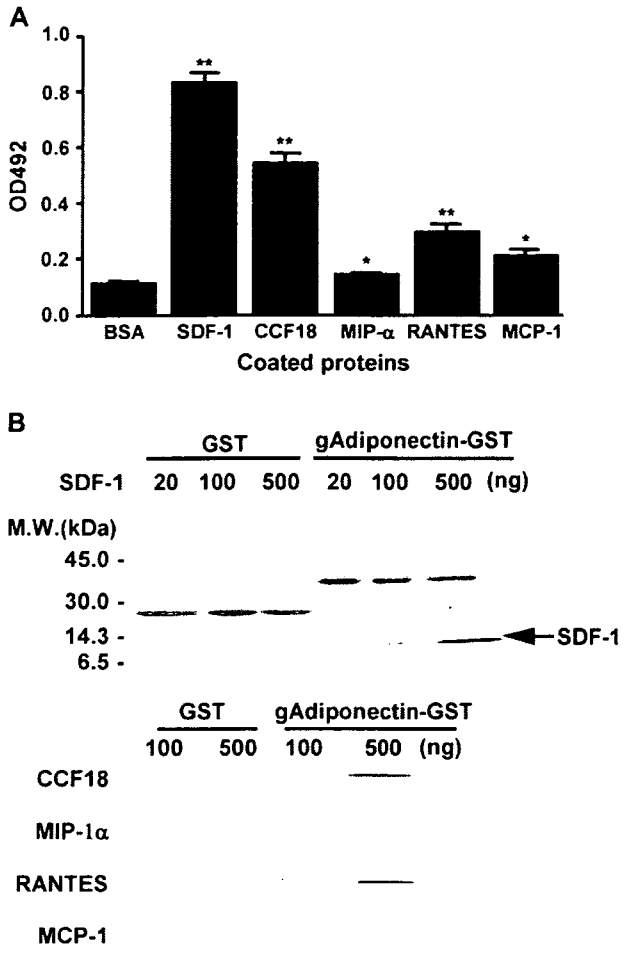

Figure 4. Adiponectin binds to various chemokines. (A) The indicated recombinant chemokine, stromal-derived factor–1 (SDF-1), CCF18, macrophage-inflammatory protein-1α (MIP-1α) , RANTES, or monocyte chemoattractant protein-1 (MCP-1; 1 μg/mL), was fixed on a microtiter tray at 4°C overnight. After blocking, recombinant adiponectin (0.5 μg/mL) was incubated at room temperature for 2 hours. The bound adiponectin was detected by mouse anti-human adiponectin antibody (ANOC9104), followed by enzyme-linked immunosorbent assay using biotinylated anti-mouse immunoglobulin (Ig) and avidin-biotin-alkaline phosphatase complex. Data are shown as means ± SD of OD_{492} in tripricated samples. Statistically differences from control values (bovine serum albumin–coated) are shown with one ($p < 0.05$) or two ($p < 0.01$) asterisks. Similar results were obtained in three independent experiments. (**B**) Recombinant gAdiponectin-glutathione-S-transferase (GST) or GST was incubated with Glutathione-Sepharose 4B for 2 hours at 4°C. The gAdiponectin-GST– or GST-bound Sepharoses was mixed with the indicated chemokine, SDF-1, CCF-18, MIP-1α, RANTES, or MCP-1 for 2 hours at 4°C, and then precipitated. The precipitates were subjected to Western blots probed with appropriate antichemokine antibody.

not detected in the precipitate with heparin (Fig. 7B). Therefore, the binding between SDF-1 and adiponectin was blocked by heparin.

These results indicate that adiponectin and heparin negatively influence each other on the binding to chemokines. This implies that the HSPG–chemokine and adiponectin–chemokine interactions may implicate each other in vivo, changing the balance in accordance with physiological condition.

Physiological roles of adiponectin in SDF-1–mediated actions

Brule et al. [18] reported that induction of MMP-9 gene expression by SDF-1 in HeLa cells depended on cell-surface HSPG, but not on CXCR4. We then analyzed effects of adiponectin on MMP-9 gene expression induced by SDF-1 (Fig. 8). Treatment of HeLa cells with SDF-1 induced MMP-9 gene expression, and this was completely inhibited by the addition of heparin. Addition of adiponectin also inhibited SDF-1–induced MMP-9 gene expression in a dose-dependent manner. Therefore, adiponectin actually modulates functional SDF-1 activity, which depends on HSPG.

SDF-1 is also critical for the homing of hematopoietic stem cells to bone marrow [22]. In bone marrow, adipocytes, but not hematopoietic cells, produce adiponectin [20]. As shown in Figure 9, serum concentration of SDF-1 is higher in adiponectin-deficient mice than controls. In addition, peripheral blood in adiponectin-deficient mice carries more hematopoietic progenitors than that in wild-type mice. Therefore, adiponectin actually influences the localization of SDF-1 in vivo.

Colocalization of adiponectin with SDF-1 at vascular walls in acute graft-vs-host disease gut

Among patients who had received bone marrow transplantation, seven patients experienced severe diarrhea. These patients were diagnosed as acute intestinal graft-vs-host disease (GVHD) from their colon biopsies. We examined the localization of adiponectin and SDF-1 in inflammatory sites. Similar staining results were obtained in all patients, and we showed representative staining data (Fig. 10). Both adiponectin and SDF-1 proteins were clearly detected at vascular walls in the gut, which were positively stained with anti-CD34 antibody. In contrast, no positive cells were observed when the sections were stained with control mouse serum. Therefore, adiponectin colocalized with SDF-1 at vascular walls in the gut of patients with acute intestinal GVHD.

Discussion

With our established two-step expression cloning strategy [14], we successfully identified SDF-1 and CCF18 as new adiponectin-binding proteins. In addition, other CC chemokines, MIP-1α, RANTES, and MCP-1 were found to associate with adiponectin while the affinity was different. Thus, adiponectin is likely to interact with various chemokines. Adiponectin could not influence the binding of SDF-1 to Jurkat cells, SDF-1–induced intracellular calcium flux, or chemotaxis, indicating that adiponectin has no effects on the interaction between SDF-1 and CXCR4 in vitro. Crump et al. [23] reported that the N-terminal eight residues of

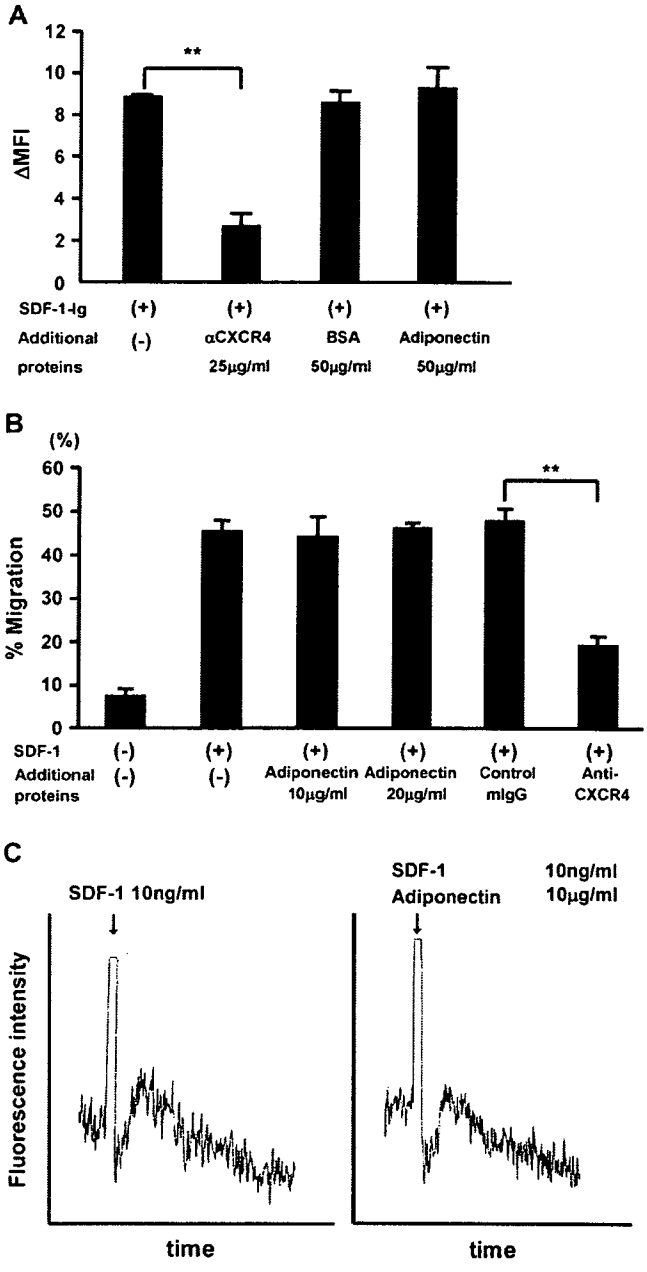

Figure 5. Adiponectin displays no influence on the stromal-derived factor–1 (SDF-1) signaling via its receptor CXCR4. (**A**) Binding of SDF-1–Ig to Jurkat cells. SDF-1-immunoglobulin (Ig) (1 μg/mL) with or without bovine serum albumin (BSA; 50 μg/mL) or adiponectin (50 μg/mL) was added to Jurkat cells (1×10^5 cells) for 20 minutes at 4°C. Jurkat cells pretreated with CXCR4 antibody (25 μg/mL) were also stained with SDF-1–Ig. After washing, the bound Ig fusion proteins were detected by fluorescein isothiocyanate–labeled anti-human Ig. Δ Mean fluorescence intensity (ΔMFI) was calculated as [MFI (the indicated staining) – MFI (control staining with second antibody alone)]. Data are shown as mean ± SD in three independent experiments. Statistically significances are shown with two ($p < 0.01$) asterisks. Similar results were obtained in three independent experiments. (**B**) SDF-1–induced chemotaxic activity. To lower wells, 300 μL RPMI-1640 medium containing SDF-1 (10 ng/mL) with or without adiponectin (10 or 20 μg/mL) was added. To upper wells, 100 μL suspension of Jurkat cells (1×10^7 cells/ml) were added. In some wells, anti-human CXCR4 antibody (5 μg/mL) or control IgG was added to upper wells. After 3 hours of incubation at 37°C, cells that migrated to the lower wells were counted. % migration was calculated as 100 × [cell number in lower wells/applied cell number]. Data are shown as mean ± SD in tripricated samples. Statistically differences from control values are shown with two ($p < 0.01$) asterisks. Similar results were obtained in two independent experiments. (**C**) SDF-1–induced Ca-influx. Fluo-3-AM–labeled Jurkat cells (1×10^6) were stimulated with the premixtures of SDF-1 (10 ng/mL) with (right) or without (left) adiponectin (10 μg/mL). The intercellular Fluo-3-AM fluorescence signals were analyzed by F-3000 fluorescence spectrophotometer. Similar results were obtained in two independent experiments.

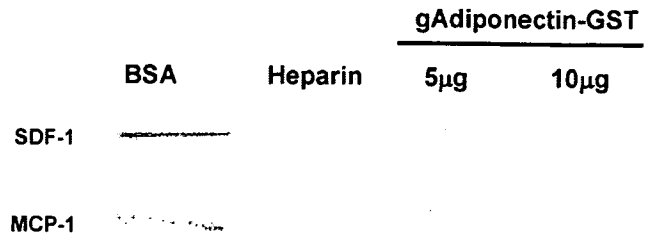

Figure 6. Adiponectin inhibits the binding of chemokines to heparin. The mixture samples of stromal-derived factor–1 (SDF-1) or monocyte chemoattractant protein-1 (MCP-1) (100 ng) and heparin Sephadex were precipitated in the presence of the indicated amount of gAdiponectin- glutathione-S-transferase (GST) or heparin (5 μg) for 2 hours at 4°C. After washing, the precipitates were subjected to Western blots probed with anti–SDF-1 or anti–MCP-1 antibody.

SDF-1, especially Lys-1 and Pro-2, formed an important receptor-binding site. Our ELISA using the deletion mutants of SDF-1 have revealed that N-terminal region of SDF-1 does not attribute to adiponectin-binding. Thus, the difference of the binding sites could be a reason why adiponectin fails to modify the interaction between SDF-1 and CXCR4. On the other hand, chemokines interact with HSPG and are immobilized on the surface of cells. The haptotactic gradient of the immobilized chemokines is essential for chemokine action in vivo, because chemokines carrying mutations in the HSPG-binding sites retained their activity in vitro, but not in vivo [21]. Because the binding of SDF-1 to heparin was significantly blocked by the presence of adiponectin, adiponectin may affect the localization of chemokines in vivo via the modification of their interactions with HSPG. Amara et al. [24] reported that the basic residues Lys-24, His-25, Lys-27, and Arg-41 of SDF-1, which cluster along the two first β strands, exhibit high positive potential to interact with HSPG. These regions correspond to the middle portion of SDF-1, which is important to bind to adiponectin. The residues responsible for the binding of the CC chemokines to HSPG are clusters of basic residues composed of Arg-18, Lys-19, Arg-24, Lys-49, Lys-58, and His-66 in MCP-1 [25,26] as well as Arg-18, Arg-46, and Arg-48 in MIP-1α [27]. The interesting result that the SDF-1–adiponectin binding was blocked by the addition

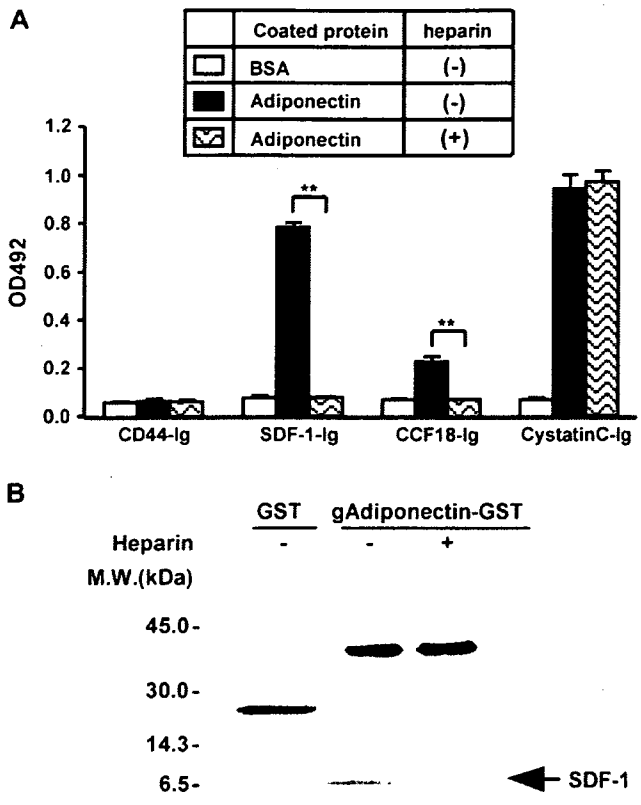

Figure 7. Heparin inhibits the binding of chemokines to adiponectin. (**A**) Recombinant adiponectin (10 μg/mL) was fixed on a microtiter tray at 4°C overnight. After blocking, stromal-derived factor-1 (SDF-1)–immunoglobulin (Ig), CCF18-Ig, or Cystatin-C–Ig (1 μg/mL) was incubated at room temperature for 2 hours in the presence or absence of heparin (10 μg/mL). The bound Ig-fusion proteins were detected with enzyme-linked immunosorbent assay using biotinylated anti-human Ig and avidin-biotin-alkaline phosophatase complex. Data are shown as mean (± SD of OD492 in tripricated samples. Statistically differences from control values are shown with two ($p < 0.01$) asterisks. Similar results were obtained in three independent experiments. (**B**) The mixture samples of SDF-1 and gAdponectin- glutathione-S-transferase (GST) glutathione Sephadex were precipitated in the presence or absence of heparin (10 μg/mL). The precipitates were subjected to Western blots probed with anti-SDF-1 antibody.

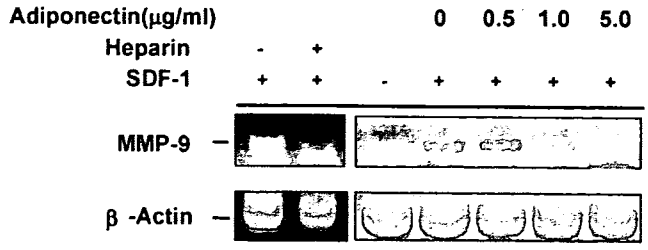

Figure 8. Adiponectin inhibits stromal-derived factor-1 (SDF-1)–induced metalloproteinase-9 (MMP-9) gene expression. HeLa cells in a confluent condition were stimulated with SDF-1 (10 ng/mL) in the presence or absence of heparin (1 μg/mL) or the indicated concentration of adiponectin for 8 hours. Total RNAs were prepared from the stimulated cells and subjected to reverse transcription polymerase chain reaction for MMP-9 or β-actin. Similar results were obtained in three independent experiments.

of heparin might suggest that adiponectin recognizes the cluster of basic residues on chemokines.

Our finding with respect to the mutual interference between heparin and adiponectin in the interaction with chemokines could be very important. It has been demonstrated that most chemokines bind to HSPG, which is ubiquitously expressed on the cell surface. This binding is thought to be functionally significant, and current models indicate that HSPG enhances the local concentration of chemokines in the vicinity of chemokine receptors [28]. Leukocyte migration along the endothelium surface and migration into the tissues at the site of inflammation is believed to depend on the local presentation of chemokines by HSPG. Homing of hematopoietic stem cells to bone marrow also depends on SDF-1, the localization of which is affected by HSPG. Our present observation raises the possibility that adiponectin might regulate chemokine-mediated functions in vivo by altering the distribution of chemokines.

In addition to antidiabetic and antiatherogenic properties [6,8], recent studies have provided insight into direct and/or indirect effects of adiponectin on inflammation. Adiponectin inhibits TNF-α–induced expression of vascular cell adhesion molecule -1 in endothelial cells [5]. Adiponectin also suppresses TNF-α–induced inflammatory changes via blocking nuclear factor-κB activation [29]. Additional anti-inflammatory effects of adiponectin include the suppression of leukocyte colony formation, the reduction of phagocytic activities and TNF-α secretion in lipopolysaccharide-stimulated macrophages as well as the enhancement of interleukin-10 production in cultured macrophages [9,30]. Indeed, an inverse relationship was observed between adiponectin and C-reactive protein in plasma of patients with coronary artery diseases [31]. Although anti-inflammatory effects of adiponectin are mediated in part by the counteraction against TNF-α, it is not clear how adiponectin itself inhibits systemic inflammation. In the present study, we found a new possible mechanism how adiponectin yields anti-inflammatory effects thorough interacting with several chemokines. Although adiponectin is abundant in plasma, it accumulates at the fatty streak in atherosclerotic lesion of apo-E–deficient mice as well as at the walls of the catheter-injured blood vessels [8,15]. Adiponectin is also found in interstitium of the infarcted lesions at an early stage of myocardial infarction [32]. We here described that adiponectin accumulates at vessel walls in the gut of patients with acute intestinal GVHD. The restricted localization of adiponectin under inflammatory circumstance could affect the distribution of chemokines. Conversely, chemokine–HSPG interactions could influence the adiponectin distribution. Further studies will give an answer to this possibility.

In summary, we identified chemokines as adiponectin-associated molecules. We clarified that the interaction occurs between the globular head of adiponectin and the central region of chemokines and that the interaction was blocked by heparin. In addition, we showed that adiponectin

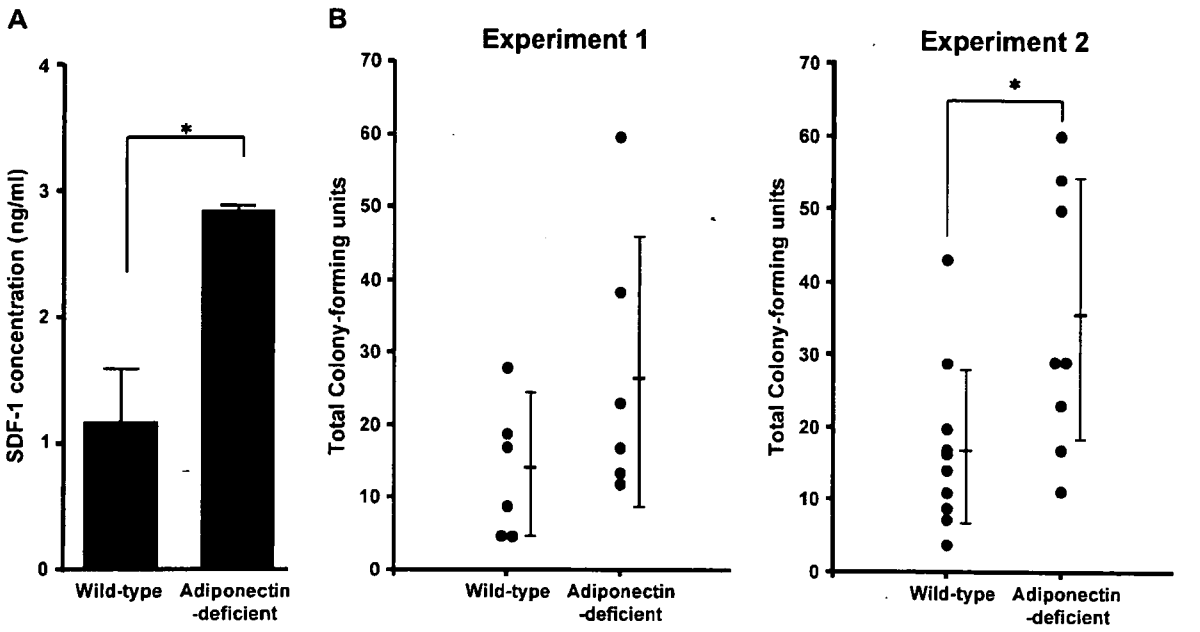

Figure 9. Adiponectin influences stromal-derived factor-1 (SDF-1) localization in vivo. Peripheral blood was collected from adiponectin-deficient or wild-type mice. (A) Serum concentration of SDF-1 was measured with Cytoscreen enzyme-linked immunosorbent assay kit. Data are shown as means (±SD in five individual mice for each group. (B) Mononuclear cells isolated from peripheral blood were subjected to colony assays for hematopoietic progenitors. Total colony numbers per 200 μL peripheral blood from each individual mice are shown. Statistically differences from control values are shown with one asterisk ($p < 0.05$).

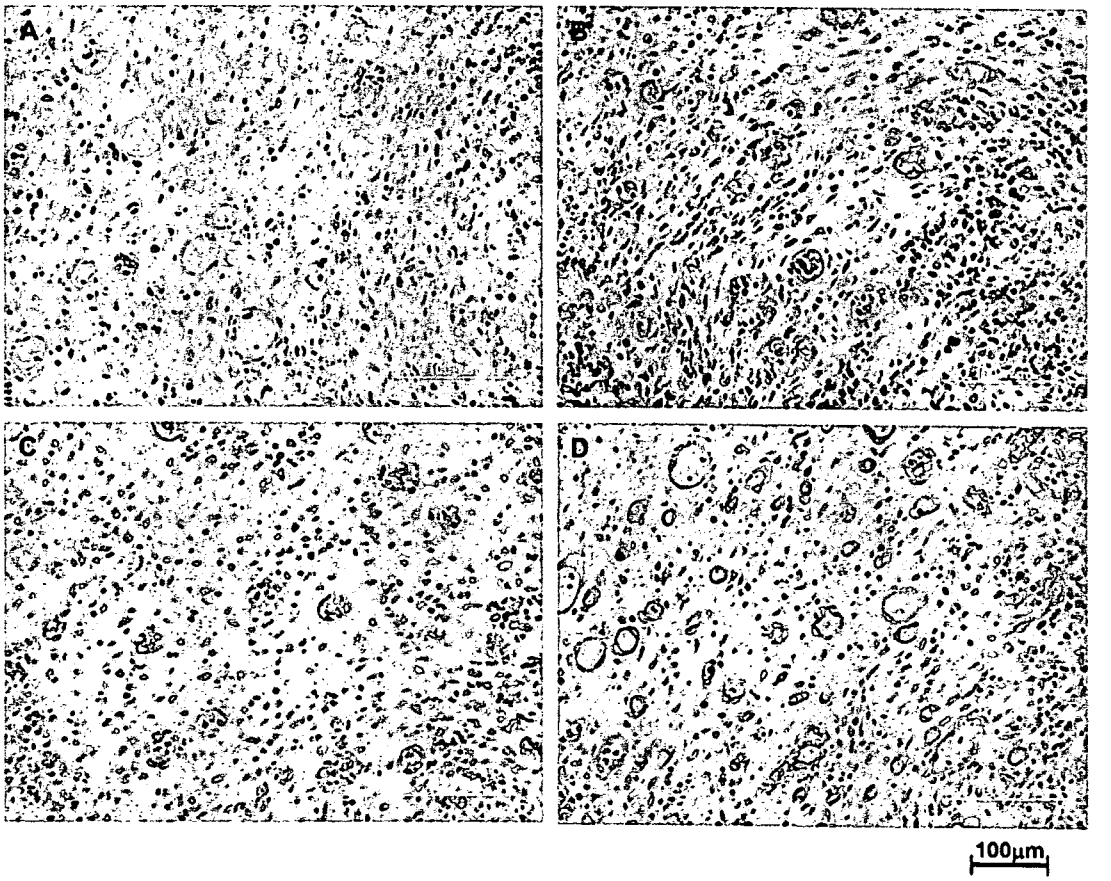

Figure 10. Localization of adiponectin and stromal-derived factor-1 (SDF-1) in guts of patients with acute intestinal graft-vs-host disease (GVHD). Colon sections from an acute intestinal GVHD patient who had received bone marrow transplantation were immunostained with control serum (A), antiadiponectin (B) or anti–SDF-1 antibody (C), or anti-CD34 antibody (D) (×200).

accumulates in inflammatory sites where the chemokines play a role in the recruitment of leukocytes. Although the physiological significance of adiponectin–chemokine interaction remains to be elucidated, our findings should give a new insight to understand how adiponectin implicates in diverse biological activities.

Acknowledgments

This work was supported in part by grants from the Japan Research Foundation for Clinical Pharmacology and the Mochida Memorial Foundation for Medical and Pharmaceutical Research.

References

1. Arita Y, Kihara S, Ouchi N, et al. Paradoxical decrease of an adipose-specific protein, adiponectin, in obesity. Biochem Biophys Res Commun. 1999;257:79–83.
2. Maeda K, Okubo K, Shimomura I, Funahashi T, Matsuzawa Y, Matsubara K. cDNA cloning and expression of a novel adipose specific collagen-like factor, apM1 (AdiPose Most abundant Gene transcript 1). Biochem Biophys Res Commun. 1996;221:286–289.
3. Shapiro L, Scherer PE. The crystal structure of a complement-1q family protein suggests an evolutionary link to tumor necrosis factor. Curr Biol. 1998;8:335–338.
4. Hotta K, Funahashi T, Arita Y, et al. Plasma concentrations of a novel, adipose-specific protein, adiponectin, in type2 diabetic patients. Arterioscler Thromb Vasc Biol. 2000;20:1595–1599.
5. Ouchi N, Kihara S, Arita Y, et al. Novel modulator for endothelial adhesion molecules. Circulation. 1999;100:2473–2476.
6. Maeda N, Shimomura I, Kishida K, et al. Diet-induced insulin resistance in mice lacking adiponectin/ACRP30. Nat Med. 2002;8:731–737.
7. Matsuda M, Shimomura I, Sata M, et al. Role of adiponectin in preventing vascular stenosis. The missing link of adipo-vascular axis. J Biol Chem. 2002;277:37487–37491.
8. Okamoto Y, Kihara S, Ouchi N, et al. Adiponectin reduces atherosclerosis in apolipoprotein E-deficient mice. Circulation. 2002;106:2767–2770.
9. Yokota T, Oritani K, Takahashi I, et al. Adiponectin, a new member of the family of soluble defense collagens, negatively regulates the growth of myelomonocytic progenitors and the functions of macrophages. Blood. 2000;96:1723–1732.
10. Yokota T, Meka CSR, Kouro T, et al. Adiponectin, a fat cell product, influences the earliest lymphocyte precursors in bone marrow cultures by activation of the cyclooxygenase-prostaglandin pathway in stromal cells. J Immunol. 2003;171:5091–5099.
11. Yamauchi T, Kamon J, Ito Y, et al. Cloning of adiponectin receptors that mediate antidiabetic metabolic effects. Nature. 2003;423:762–769.
12. Wang Y, Lam KSL, Xu JY, et al. Adiponectin inhibits cell proliferation by interacting with several growth factors in an oligomerization-dependent manner. J Biol Chem. 2005;280:18341–18347.
13. Hug C, Wang J, Ahmad NS, Bogan JS, Tsao TS, Lodish HF. T-cadherin is a receptor for hexameric and high-molecular-weight forms of Acrp30/adiponectin. Proc Natl Acad Sci. 2004;101:10308–10313.
14. Oritani K, Kincade PW. Identification of stromal cell products that interact with Pre-B cells. J Cell Biol. 1996;134:771–782.
15. Nagasawa T, Kikutani H, Kishimoto T. Molecular cloning and structure of a pre-B-cell growth-stimulating factor. Proc Natl Acad Sci USA. 1994;91:2305–2309.
16. Hara T, Bacon KB, Cho LC, et al. Molecular cloning and functional characterization of a novel member of the C-C chemokine family. J Immunol. 1995;155:5352–5358.
17. Roland J, Murphy BJ, Ahr B, et al. Role of the intracellular domains of CXCR4 in SDF-1-mediated signaling. Blood. 2003;101:399–406.
18. Brule S, Charnaux N, Sutton A, et al. The shedding of syndecan-4 and syndecan-1 from Hela cells and human primary macrophages is accelerated by SDF-1/CXCL12 and mediated by the matrix metalloproteinase-9. Glycobiology. 2006;16:488–501.
19. Okamoto Y, Arita Y, Nishida M, et al. An adipocyte-derived plasma protein, adiponectin, adheres to injured vascular walls. Horm Metab Res. 2000;32:47–50.
20. Yokota T, Meka CSR, Medina KL, et al. Paracrine regulation of fat cell formation in bone marrow cultures via adiponectin and prostaglandins. J Clin Invest. 2002;109:1303–1310.
21. Proudfoot AEI, Handel TM, Johnson Z, et al. Glycosaminoglycan binding and oligomerization are essential for the in vivo activity of certain chemokines. Proc Natl Acad Sci U S A. 2003;100:1885–1890.
22. Aiuti A, Webb IJ, Bleul C, et al. The chemokine SDF-1 is a chemoattractant for human CD34+ hematopoietic progenitor cells and provides a new mechanism to explain the mobilization of CD34+ progenitors to peripheral blood. J Exp Med. 1997;185:111–120.
23. Crump MP, Gong JH, Loetscher P, et al. Solution structure and basis for functional activity of stromal cell-derived factor-1; dissociation of CXCR4 activation from binding and inhibition of HIV-1. EMBO J. 1997;16:6996–7007.
24. Amara A, Lorthioir O, Valenzuela A, et al. Stromal cell-derived factor-1 alpha associates with heparan sulfates through the first beta-strand of the chemokine. J Biol Chem. 1999;274:23916–23925.
25. Lau EK, Paavola CD, Johnson Z, et al. Identification of the glycosaminoglycan binding site of the CC chemokine, MCP-1: implications for structure and function in vivo. J Biol Chem. 2004;279:22294–22305.
26. Chakravarty L, Rogers L, Quach T, Breckenridge S, Kolattukudy PE. Lysine 58 and histidine 66 at the C-terminal alpha-helix of monocyte chemoattractant protein-1 are essential for glycosaminoglycan binding. J Biol Chem. 1998;273:29641–29647.
27. Koopmann W, Krangel MS. Identification of a glycosaminoglycan-binding site in chemokine macrophage inflammatory protein-1 alpha. J Biol Chem. 1997;272:10103–10109.
28. Hoogewerf AJ, Kuschert GSV, Proudfoot AEI, et al. Glycosaminoglycans mediate cell surface oligomerization of chemokines. Biochemistry. 1997;36:13570–13578.
29. Ouchi N, Kihara S, Arita Y, et al. Adiponectin, an-adipocyte-derived plasma protein, inhibits endothelial NF-kB signaling through a cAMP-dependent pathway. Circulation. 2000;102:1296–1301.
30. Kumada M, Kihara S, Ouchi N, et al. Adiponectin specifically increased tissue inhibitor of matelloproteinase-1 through interleukin-10 expression in human macrophages. Circulation. 2004;109:2046–2049.
31. Ouchi N, Kihara S, Funahashi T, et al. Reciprocal association of C-reactive protein with adiponectin in blood stream and adipose tissue. Circulation. 2003;107:671–674.
32. Ishikawa Y, Akasaka Y, Ishii T, et al. Changes in the distribution pattern of gelatin-binding protein of 28 kDa (adiponectin) in myocardial remodelling after ischaemic injury. Histopathology. 2003;42:43–52.

Brief report

Functional imaging of shear-dependent activity of ADAMTS13 in regulating mural thrombus growth under whole blood flow conditions

Yasuaki Shida,[1] Kenji Nishio,[2] Mitsuhiko Sugimoto,[1] Tomohiro Mizuno,[1] Masaaki Hamada,[1] Seiji Kato,[3] Masanori Matsumoto,[3] Kazuo Okuchi,[2] Yoshihiro Fujimura,[3] and Akira Yoshioka[1]

Departments of [1]Pediatrics, [2]Emergency and Critical Care Medicine, and [3]Blood Transfusion Medicine, Nara Medical University, Kashihara, Nara, Japan

The metalloprotease ADAMTS13 is assumed to regulate the functional levels of von Willebrand factor (VWF) appropriate for normal hemostasis in vivo by reducing VWF multimer size, which directly represents the thrombogenic activity of this factor. Using an in vitro perfusion chamber system, we studied the mechanisms of ADAMTS13 action during platelet thrombus formation on a collagen surface under whole blood flow conditions. Inhibition studies with a function-blocking anti-ADAMTS13 antibody, combined with immunostaining of thrombi with an anti-VWF monoclonal antibody that specifically reflects the VWF-cleaving activity of ADAMTS13, provided visual evidence for a shear rate–dependent action of ADAMTS13 that limits thrombus growth directly at the site of the ongoing thrombus generation process. Our results identify an exquisitely specific regulatory mechanism that prevents arterial occlusion under high shear rate conditions during mural thrombogenesis. (Blood. 2008; 111:1295-1298)

Introduction

The adhesive protein von Willebrand factor (VWF) plays a major role in platelet thrombogenesis, a process crucial for hemostasis. However, the excessive function of VWF is thought to increase the risk of fatal arterial thrombosis.[1,2] The thrombogenic activity of VWF is strictly dependent upon its multimeric structure, which is thought to be regulated in vivo by the metalloprotease ADAMTS13 through its cleavage of the A2 domain of the VWF subunit.[3,4] Indeed, patients with congenital deficiency of ADAMTS13 suffer repeated thrombotic complications attributed to excessive function of the ultra-large VWF (ULVWF) multimer, which is not found in normal blood circulation.[3-6] This concept was recently confirmed by knock-out mouse studies, in which ADAMTS13$^{-/-}$ mice exhibited enhanced thrombogenicity in the ex vivo or in vitro experimental blood flow conditions tested.[7,8]

The mechanisms by which ADAMTS13 regulates VWF remain poorly understood. However, recent studies showing that ADAMTS13 under flow conditions can rapidly cleave ULVWF secreted from and anchored to cultured endothelial cell layers[9,10] have raised the possibility that blood flow is critical in activating ADAMTS13.[11] Indeed, the VWF-cleaving activity of ADAMTS13 cannot be reproduced in vitro under static conditions unless the substrate VWF molecule is somewhat modified (eg, denatured by guanidine-HCl or urea).[3,4] Further, the question arises of whether ADAMTS13, in addition to its known action on ULVWF freshly released from endothelial cells, might also act directly at the local sites of thrombus generation to regulate thrombus growth.

To address these issues, we analyzed the role and mechanisms of ADAMTS13 action in mural platelet thrombogenesis on a collagen-coated glass surface in an in vitro perfusion chamber system. Our visual evidence demonstrates that ADAMTS13 cleaves VWF and down-regulates mural thrombus growth at the site of ongoing thrombus generation in a shear rate–dependent manner under whole blood flow conditions.

Methods

Blood collection

The present work was approved by the institutional review board of Nara Medical University, and informed consent was obtained in accordance with the Declaration of Helsinki. Using 200 μM argatroban as an anticoagulant, blood was collected from 10 nonsmoking healthy volunteers who had not taken any medications in the previous 2 weeks.

Monoclonal antibodies

A function-blocking anti-ADAMTS13 monoclonal antibody (A10), which completely inhibits plasma ADAMTS13 activity at the concentration of 20 μg/mL,[12] was used as a divalent $(ab')_2$ fragment in inhibition studies. An anti-VWF monoclonal antibody (N10) was used that reacts with an epitope within the VWF A2 domain (10-amino acid VWF peptide; D^{1596}REQAPNLVY^{1605}) only after cleavage by ADAMTS13 exposes the epitope; thus, reactivity of antibody N10 specifically reflects the VWF-cleaving activity of ADAMTS13, as described.[13]

Submitted September 2, 2007; accepted October 3, 2007. Prepublished online as *Blood* First Edition paper, October 10, 2007; DOI 10.1182/blood-2007-09-110700.

An Inside *Blood* analysis of this article appears at the front of this issue.

The publication costs of this article were defrayed in part by page charge payment. Therefore, and solely to indicate this fact, this article is hereby marked "advertisement" in accordance with 18 USC section 1734.

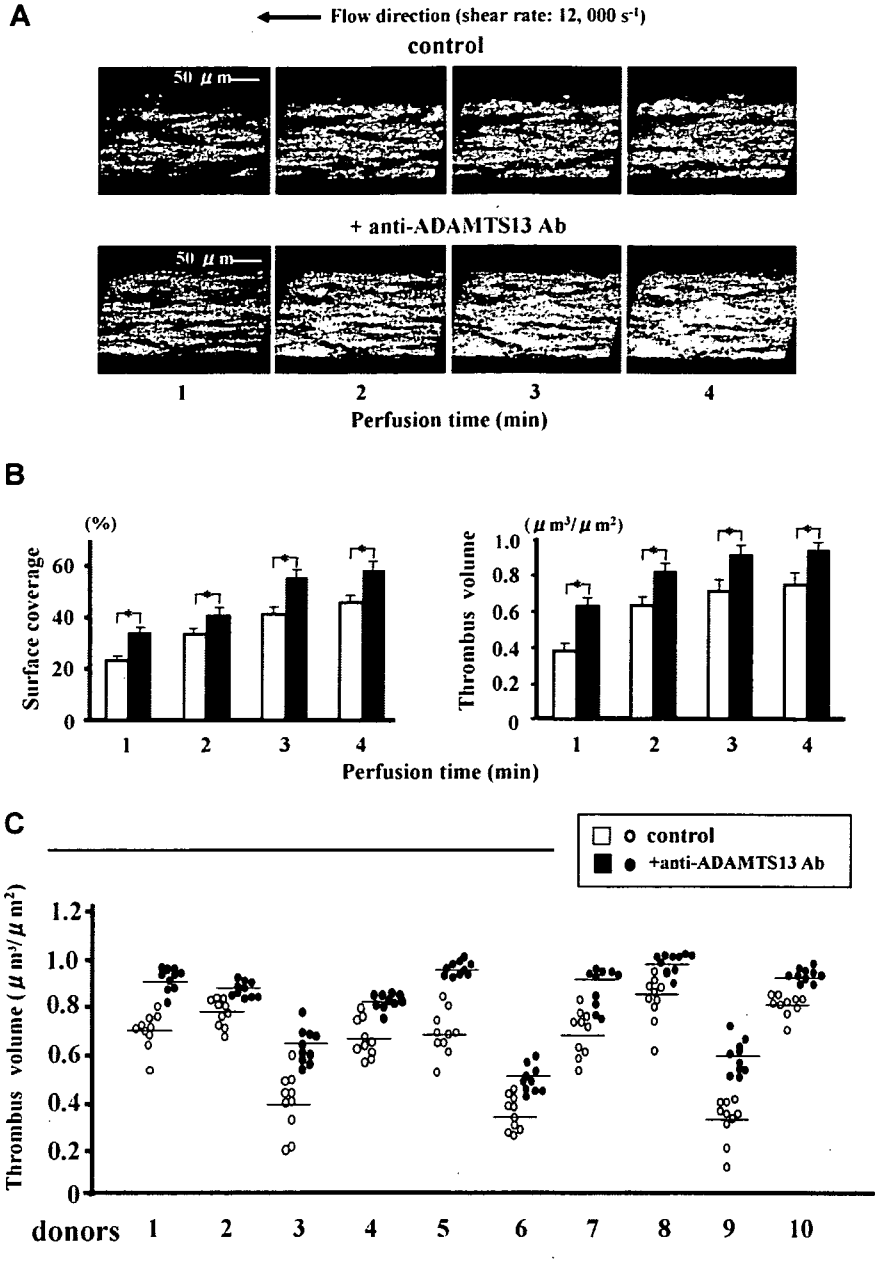

Figure 1. Effects of a function-blocking anti-ADAMTS13 monoclonal antibody (A10) on mural thrombus generation under very high shear rate conditions. Whole blood from healthy volunteers containing DiOC6 (1 μM)-labeled platelets, anticoagulated with argatroban, was perfused over a type I collagen-coated glass surface under very high shear rate (12 000 s^{-1}) with anti-ADAMTS13 antibody A10 or with control mouse IgG (each 20 μg/mL). (A) Time-course changes of 3-dimensional images of thrombi (original magnification, ×600), which were constructed by the image-analyzing system of confocal laser scanning microscopy (CLSM) based on successive horizontal slices at identical portions, are representative of 10-pair flow experiments using blood from 10 independent donors. (B) Statistical analyses corresponding to the above images; bars represent mean (+ SD) surface coverage or total thrombus volume in 10 areas (each 133 × 100 μm) randomly selected in each perfusion using a single donor blood (donor number 1 in panel C). Note that thrombus generation is significantly (*; $P < .01$) accelerated in the presence of the anti-ADAMTS13 antibody. (C) Thrombus volume at 3 minutes' perfusion in 10-pair flow experiments using 10 independent donors; data points represent values of 10 areas randomly selected in each perfusion with (●) or without (○) anti-ADAMTS13 antibody, and transverse lines indicate mean values for each group. Note also that thrombus volumes generated in the presence of anti-ADAMTS13 antibody are significantly ($P < .01$; asterisks not included in the figure) greater than control thrombi in all 10-pair experiments.

In vitro perfusion studies

Thrombus generation on a type I collagen-coated (Sigma-Aldrich, Tokyo, Japan) glass surface was studied under various shear rates in a parallel plate flow chamber system as described.[14-17] Surface coverage and volume of thrombi generated at the indicated time points during whole blood perfusion were evaluated based on images obtained by confocal laser scanning microscopy (CLSM; FV300; Olympus, Tokyo, Japan), as described.[15-17] Immunohistochemical staining of thrombi using anti-VWF antibodies was performed as described.[15-17] Briefly, thrombi on a glass surface were fixed with paraformaldehyde and incubated with a mixture of anti–whole VWF rabbit polyclonal antibody (30 μg/mL; DAKO Cytomation, Kyoto, Japan) and N10 antibody (60 μg/mL) or with the negative control IgG mixture (rabbit; 30 μg/mL, mouse; 60 μg/mL; DAKO Cytomation) for 90 minutes at 37°C. Samples were then stained with a mixture of fluorescein isothiocyanate (FITC)–conjugated anti–rabbit IgG (3.3 μg/mL; BioSource International, Camarillo, CA) and Cy3-conjugated anti–mouse IgG (3.3 μg/mL; Sigma-Aldrich) as secondary fluorescent antibodies for 90 minutes at 37°C. and viewed by CLSM. These conditions were determined in preliminary experiments to confirm the sufficient infiltration of both primary and secondary fluorescent antibodies into thrombi.

Results and discussion

To address the potential role of ADAMTS13 in the ongoing process of mural thrombus generation, we compared the size of thrombi generated in the presence or absence of a function-blocking antibody against ADAMTS13 in a perfusion chamber system, using blood from the same donor. This relatively simple experimental approach is able to precisely evaluate ADAMTS13 function in uniform blood conditions, avoiding the individual heterogeneity of sample blood conditions including VWF and platelets that might otherwise seriously affect the size of thrombi generated in this type of flow experiment.

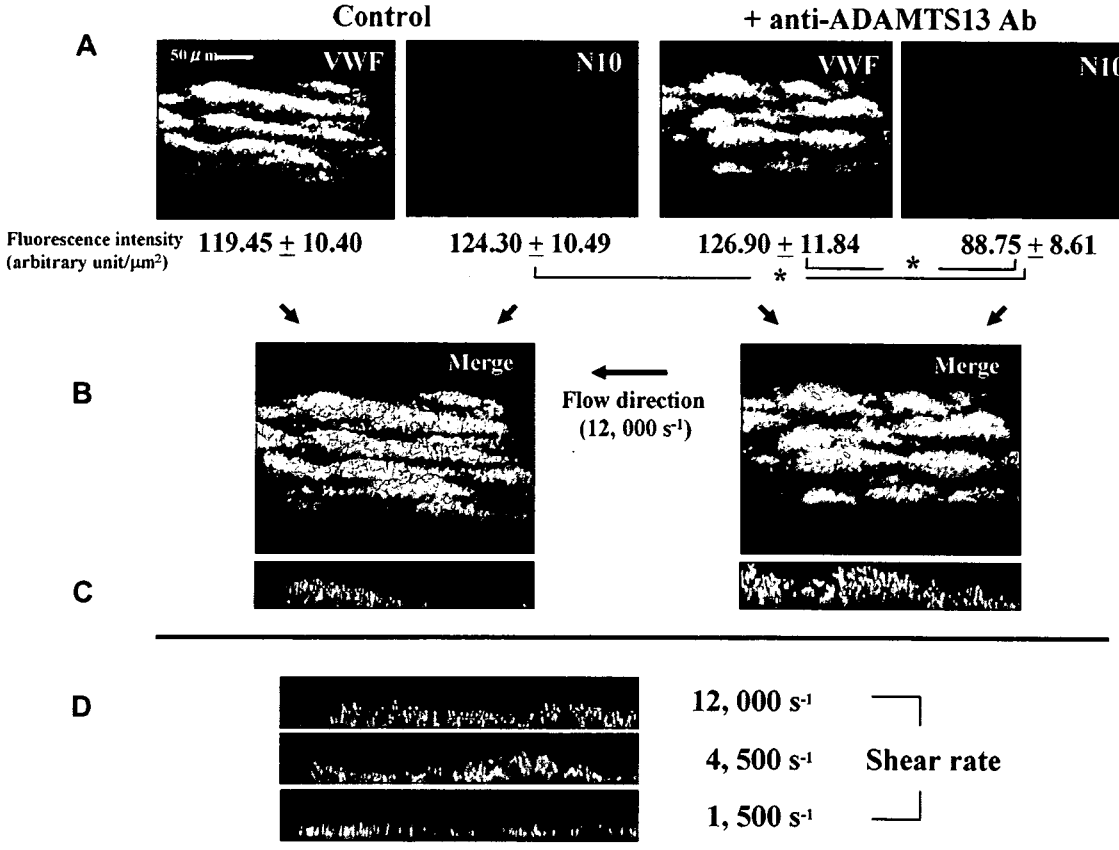

Figure 2. Visual evaluation of ADAMTS13 activity within thrombi generated under high shear rate conditions using a monoclonal antibody (N10) that specifically detects ADAMTS13-cleaved VWF. Experimental conditions were as described in Figure 1, except that platelets were not labeled. Thrombi generated on a collagen-coated glass surface at 3 minutes' perfusion with or without an anti-ADAMTS13 antibody under 12 000 s^{-1} shear were fixed, reacted with both N10 antibody and anti–whole VWF antibody, double-stained with Cy3 (red)- and FITC (green)-fluorescence, and viewed by CLSM. (A) Three-dimensional images of thrombi, representative of 5 independent flow experiments, and the corresponding fluorescence intensity (mean ± SD of 5 areas randomly selected in a single perfusion) corrected for background value (negative control IgGs), indicate that VWF cleavage by ADAMTS13 (red color) within thrombi is significantly (*; $P < .01$) reduced in the presence of anti-ADAMTS13 antibody as compared with control thrombi (original magnification; ×600). (B) Merged 3-dimensional images and (C) the corresponding longitudinal views of thrombi; in the merged images, portions stained with both green and red fluorescence basically show the color of the higher pixel value, whereas a yellowish color is seen when both pixel values are nearly equal. Thus, the predominantly reddish appearance of the surface portions of control thrombi suggests that ADAMTS13 is more active on the surface of thrombi forming under very high shear rate conditions, while this tendency is barely visible in the presence of anti-ADAMTS13 antibody. (D) Longitudinal views of thrombi, generated at 3 minutes' perfusion without an anti-ADAMTS13 antibody under various shear rates and double-stained, are representative of 5 separate experiments. Note the prominent red color, especially at the surface portions of thrombi, indicating higher ADAMTS13 activity under higher shear rates.

Under a very high shear rate of 12 000 s^{-1}, thrombus growth was significantly accelerated by addition of anti-ADAMTS13 antibody (Figure 1). This enhanced thrombogenesis most likely reflects a block in ADAMTS13 activity rather than nonspecific effects of antibody on platelets, since immunostaining of thrombi with N10 antibody, which reacts only with VWF cleaved by ADAMTS13, visually confirmed the reduced VWF cleavage within thrombi by the anti-ADAMTS13 antibody (Figure 2A). Thus, these results clearly point to the regulatory role of ADAMTS13 during thrombus generation.

While the preceding observations were made under a much higher shear rate than the high shear rate typically used in platelet functional studies (ie, 1500 s^{-1} in our laboratory[14-16]), similar observations, although less pronounced, were confirmed under lower shear rates (Figure 2D). In addition, longitudinal views of thrombi revealed the preferential VWF-cleavage activity of ADAMTS13 at the surface portions of forming thrombi during thrombogenesis (Figure 2B,C). The thrombus surface is thought to directly encounter blood flow with the highest shear rate under such flow circumstances, where the wall shear rate can increase as the flow path narrows in parallel with thrombus growth.[15] Together, these observations strongly suggest a shear rate–dependent property of ADAMTS13 function.

Shear forces are thought to transform the globular conformation of the immobilized VWF multimer observed under static conditions to a shape resembling a spreading bird wing, consistent with the shear rate–dependent acceleration of the VWF-glycoprotein Ib interaction under high shear.[18] By analogy, a stretching of the VWF multimeric structure by shear forces may also be critical for the action of ADAMTS13 in exposing the latent reactive site on the VWF molecule. In this regard, increased tensile strength of the VWF multimeric structure on binding to platelets might augment the stretching effects of shearing forces, resulting in up-regulated ADAMTS13 activity.[19,20] This possibility seems compatible with recent findings indicating that even under low shear rate conditions, ADAMTS13 can cleave ULVWF released from endothelial cells,[9,10] because a greater number of platelets can bind spontaneously to ULVWF as compared with normal-sized VWF without shearing forces.

The mechanisms described here represent an exquisite orchestration by platelets, VWF, and ADAMTS13 under high shear to properly regulate the final size of mural thrombi in vivo and

prevent excessive thrombogenesis from occluding the vessel lumen. Because ADAMTS13 activity appears to be triggered in response to the increased local shear rate associated with the development of thrombi, our results may provide a novel avenue toward strategies that prevent arterial thrombosis without bleeding complications.

Acknowledgments

We thank Marina Hoffman for editorial assistance.

This work was supported in part by Ministry of Education, Culture, Sports, Science and Technology of Japan grants 15390305 and 19591129 (M.S.), 19592095 (K.N.), and 17390304 (A.Y.), and by the Ministry of Health and Welfare of Japan (M.S.) for Clinical Research of Myocardial Infarction, Stroke and Diabetes Mellitus.

Authorship

Contribution: Y.S. performed most of the flow experiments, data analysis, and the manuscript preparation; T.M. and M.H. helped perform the flow experiments and data analysis; S.K., M.M., and Y.F. produced and characterized monoclonal antibodies; A.Y. and K.O. provided direction throughout the work and helped prepare the manuscript; and M.S. and K.N. provided the overall experimental designs and direction of this work, and prepared the manuscript.

Conflict-of-interest disclosure: The authors declare no competing financial interests.

Correspondence: Mitsuhiko Sugimoto, MD, or Kenji Nishio Department of Pediatrics, Nara Medical University, 840 Shijo-cho, Kashihara, Nara 634-8522, Japan; e-mail: sugi-ped@naramed-u.ac.jp. or knishio@naramed-u.ac.jp.

References

1. Sadler JE. von Willebrand factor: two sides of a coin. J Thromb Haemost. 2005;3:1702-1709.
2. Tsai HM. Shear stress and von Willebrand factor in health and disease. Semin Thromb Hemost. 2003;29:479-488.
3. Furlan M. Deficient activity of von Willebrand factor-cleaving protease in thrombotic thrombocytopenic purpura. Expert Rev Cardiovasc Ther. 2003;1:243-255.
4. Lammle B, George JN. Thrombotic thrombocytopenic purpura: advances in pathophysiology, diagnosis, and treatment–introduction. Semin Hematol. 2004;41:1-3.
5. Levy GG, Nichols WC, Lian EC, et al. Mutations in a member of the ADAMTS gene family cause thrombotic thrombocytopenic purpura. Nature. 2001;413:488-494.
6. Tsai HM. Deficiency of ADAMTS13 and thrombotic thrombocytopenic purpura. Blood. 2002; 100:3839-3840; author reply 3840-3842.
7. Chauhan AK, Motto DG, Lamb CB, et al. Systemic antithrombotic effects of ADAMTS13. J Exp Med. 2006;203:767-776.
8. Banno F, Kokame K, Okuda T, et al. Complete deficiency in ADAMTS13 is prothrombotic, but it alone is not sufficient to cause thrombotic thrombocytopenic purpura. Blood. 2006;107:3161-3166.
9. Dong JF, Moake JL, Bernardo A, et al. ADAMTS-13 metalloprotease interacts with the endothelial cell-derived ultra-large von Willebrand factor. J Biol Chem. 2003;278:29633-29639.
10. Dong JF. Cleavage of ultra-large von Willebrand factor by ADAMTS-13 under flow conditions. J Thromb Haemost. 2005;3:1710-1716.
11. Donadelli R, Orje JN, Capoferri C, Remuzzi G, Ruggeri ZM. Size regulation of von Willebrand factor-mediated platelet thrombi by ADAMTS13 in flowing blood. Blood. 2006;107:1943-1950.
12. Uemura M, Tatsumi K, Matsumoto M, et al. Localization of ADAMTS13 to the stellate cells of human liver. Blood. 2005;106:922-924.
13. Kato S, Matsumoto M, Matsuyama T, Isonishi A, Hiura H, Fujimura Y. Novel monoclonal antibody-based enzyme immunoassay for determining plasma levels of ADAMTS13 activity. Transfusion. 2006;46:1444-1452.
14. Tsuji S, Sugimoto M, Miyata S, Kuwahara M, Kinoshita S, Yoshioka A. Real-time analysis of mural thrombus formation in various platelet aggregation disorders: distinct shear-dependent roles of platelet receptors and adhesive proteins under flow. Blood. 1999;94:968-975.
15. Matsui H, Sugimoto M, Mizuno T, et al. Distinct and concerted functions of von Willebrand factor and fibrinogen in mural thrombus growth under high shear flow. Blood. 2002;100:3604-3610.
16. Sugimoto M, Matsui H, Mizuno T, et al. Mural thrombus generation in type 2A and 2B von Willebrand disease under flow conditions. Blood. 2003;101:915-920.
17. Mizuno T, Sugimoto M, Matsui H, Hamada M, Shida Y, Yoshioka A. Visual evaluation of blood coagulation during mural thrombogenesis under high shear flow. Thromb Res. 2007; Sep 25 [Epub ahead of print].
18. Siedlecki CA, Lestini BJ, Kottke-Marchant KK, Eppell SJ, Wilson DL, Marchant RE. Shear-dependent changes in the three-dimensional structure of human von Willebrand factor. Blood. 1996;88:2939-2950.
19. Nishio K, Anderson PJ, Zheng XL, Sadler JE. Binding of platelet glycoprotein Ibalpha to von Willebrand factor domain A1 stimulates the cleavage of the adjacent domain A2 by ADAMTS13. Proc Natl Acad Sci U S A. 2004;101:10578-10583.
20. Gao W, Anderson PJ, Majerus EM, Tuley EA, Sadler JE. Exosite interactions contribute to tension-induced cleavage of von Willebrand factor by the antithrombotic ADAMTS13 metalloprotease. Proc Natl Acad Sci U S A. 2006;103:19099-19104.

Volume 56(2): 175–182, 2008
Journal of Histochemistry & Cytochemistry
http://www.jhc.org

ARTICLE

Differential Expression Patterns of NDRG Family Proteins in the Central Nervous System

Tomohiko Okuda, Koichi Kokame, and Toshiyuki Miyata

National Cardiovascular Center Research Institute, Osaka, Japan

SUMMARY The N-myc downstream-regulated gene (NDRG) family consists of four proteins: NDRG1, NDRG2, NDRG3, and NDRG4 in mammals. NDRG1 has been thoroughly studied as an intracellular protein associated with stress response, cell growth, and differentiation. A nonsense mutation in the NDRG1 gene causes hereditary motor and sensory neuropathy, Charcot–Marie–Tooth disease type 4D. We previously generated *Ndrg1*-deficient mice and found that they exhibited peripheral nerve degeneration caused by severe demyelination, but that the complicated motor abilities were retained. These results implied that other NDRG family proteins may compensate for the NDRG1 deficiency in the central nervous system. In this study we raised specific antibodies against each member of the NDRG protein family and examined their cellular expression patterns in the mouse brain. In the cerebrum, NDRG1 and NDRG2 were localized in oligodendrocytes and astrocytes, respectively, whereas NDRG3 and NDRG4 were ubiquitous. In the cerebellum, NDRG1 and NDRG4 were localized in Purkinje cells and NDRG2 in Bergmann glial cells. NDRG3 was detected in the nuclei in most cells. These expression patterns demonstrated the cell type-specific and ubiquitous localization of the NDRG family proteins. Each NDRG may play a partially redundant role in specific cells in the brain. (J Histochem Cytochem 56:175–182, 2008)

KEY WORDS
NDRG1
NDRG2
NDRG3
NDRG4
brain
Charcot–Marie–Tooth disease
oligodendrocyte
astrocyte
immunohistochemistry

THE N-myc downstream-regulated gene (NDRG) family consists of four proteins: NDRG1, NDRG2, NDRG3, and NDRG4 in mammals. They are intracellular proteins of 340 to 394 amino acids and share 53 to 65% sequence identities to each other (Okuda and Kondoh 1999; Zhou et al. 2001; Qu et al. 2002). Among this family of proteins, NDRG1 has been thoroughly studied as an inducible protein by a number of stress and pathological conditions (Kovacevic and Richardson 2006). *NDRG1* was first identified as a stress stimuli-induced gene (Kokame et al. 1996; Zhou et al. 1998). It was also reported as a downregulated gene in tumors (van Belzen et al. 1997), regulated by p53 (Kurdistani et al. 1998; Stein et al. 2004), associated with the differentiation and malignant states of cancers (Piquemal et al. 1999; Xu et al. 1999; Guan et al. 2000; Bandyopadhyay et al. 2003), and regulated by *N-myc* (Shimono et al. 1999).

Correspondence to: Toshiyuki Miyata, PhD, National Cardiovascular Center Research Institute, 5-7-1 Fujishirodai, Suita, Osaka 565-8565, Japan. E-mail: miyata@ri.ncvc.go.jp

Received for publication July 24, 2007; accepted October 22, 2007 [DOI: 10.1369/jhc.7A7323.2007].

NDRG1 is the gene responsible for Charcot–Marie–Tooth disease type 4D (CMT4D), also called hereditary motor and sensory neuropathy-Lom (Kalaydjieva et al. 1996,2000). Patients exhibit early-onset peripheral neuropathy, which progresses in adulthood to severe disability characterized by muscle weakness, sensory loss, and neural deafness. Diseases caused by deficiency of NDRG2, NDRG3, or NDRG4 have not yet been identified. Although studies about the NDRG family proteins have been accumulating, their molecular functions are still elusive.

To clarify the physiological roles of NDRG1, we generated *Ndrg1*-deficient mice and analyzed their phenotypes (Okuda et al. 2004). They exhibited a progressive demyelinating disorder of the peripheral nerves. Sporadic demyelination began by 5 weeks of age in the sciatic nerve, whereas the proliferation of Schwann cells and initial myelination were normal for 2 weeks after birth. In wild-type mice, NDRG1 was abundantly expressed in the cytoplasm of Schwann cells rather than in the myelin sheaths. Therefore, NDRG1 deficiency leads to autonomous dysfunction of Schwann cells, resulting in demyelination in peripheral nerves. This suggests that NDRG1 is essential for the maintenance of

0022-1554/07/$3.30

myelin sheaths in peripheral nerves. In contrast to muscle weakness caused by peripheral nerve degeneration, the complicated motor abilities in *Ndrg1*-deficient mice were relatively retained. These results suggest that functional compensation for NDRG1 deficiency may exist in the central nervous system (CNS).

Transcripts of NDRG1, NDRG2, NDRG3, and NDRG4 have been detected in the brain (Zhou et al. 2001; Okuda et al. 2004). In the present study we raised specific antibodies against each member of NDRGs and examined their expression patterns in the mouse CNS by immunohistochemical analysis. We found the cell type-specific and ubiquitous localization of NDRGs.

Materials and Methods

Animals

Adult male mice (C57BL/6 Cr Slc) aged 8 to 12 weeks (Japan SLC Inc.; Hamamatsu, Japan) were used in this study. Adult or 4-week-old *Ndrg1*-deficient male mice (Okuda et al. 2004) were also used. Mice were bred at a controlled temperature (22C) and lighting (lights on at 8 AM and off at 8 PM) for at least 1 week. Animal experiments were conducted in accordance with the guidelines for the care and use of experimental animals of the National Cardiovascular Center in Japan.

Antibodies and Vectors

Rabbit polyclonal anti-human NDRG1 and anti-human NDRG4 antibodies were raised against bacterial recombinant glutathione S-transferase-fusion proteins of NDRG1 and NDRG4, respectively, and purified by the fusion protein-immobilized affinity column chromatography (Agarwala et al. 2000; Zhou et al. 2001). Rabbit polyclonal anti-NDRG2 and anti-NDRG3 antibodies were raised against the following synthetic peptides conjugated with keyhole limpet hemocyanin and purified by peptide-immobilized affinity column chromatography: Q^{351}SSESGTLPSGPPGH^{365} for mouse NDRG2 and F^{343}SRSVTSNQSDGTQE^{357} for mouse NDRG3. The mouse monoclonal anti-2′,3′-cyclic nucleotide 3′-phosphodiesterase (CNPase) antibody (clone 11-5B) was purchased from Sigma-Aldrich (St Louis, MO). Mouse monoclonal anti-glial fibrillary acidic protein (GFAP) antibody and mouse monoclonal anti-neuronal nuclei (NeuN) antibody were purchased from Chemicon (Temecula, CA).

Expression vectors for the green fluorescent protein (GFP)-fusion proteins of mouse NDRG1, NDRG2, NDRG3, and NDRG4 were constructed with the pEGFP-N1 vector (Clontech; Mountain View, CA). COS-1 cells were transfected with these vectors using the FuGENE6 transfection reagent (Roche Diagnostics; Indianapolis, IN). Two days later, cells were collected and lysed with lysis buffer (10 mM Tris–HCl, 2 mM EDTA, 50 mM dithiothreitol, 2% SDS, 6% glycerol, pH 6.8).

Western Blotting Analysis

The excised whole brain was homogenized in the lysis buffer. Protein lysates were subjected to SDS-PAGE (10–20% gradient gel; Daiichi Pure Chemicals, Tokyo, Japan) and transferred to a polyvinylidene difluoride membrane (Bio-Rad; Hercules, CA). An equal amount of loading of the protein samples was confirmed by using the RC DC protein assay kit (Bio-Rad). After blocking with 3% skim milk in PBS with 0.05% Tween-20, the membrane was incubated with 0.5-μg/ml antibodies and then with a 1:1000 dilution of peroxidase-conjugated goat anti-rabbit IgG (Zymed; South San Francisco, CA). Chemiluminescent signals were developed using Western Lightning Chemiluminescence Reagent Plus (PerkinElmer Life Sciences; Wellesley, MA) and detected by an image analyzer LAS-1000plus (Fuji Film; Tokyo, Japan).

Histological Analyses

Mice (8–12 weeks old) were anesthetized with Nembutal (Abbott Laboratories; North Chicago, IL) and perfused with ice-cold 4% paraformaldehyde in PBS. Brain was then excised and fixed in 4% paraformaldehyde in PBS overnight at 4C. For light microscopy, specimens were embedded in paraffin by standard procedures. Four-μm-thick paraffin sections were stained with hematoxylin–eosin or luxol–fast blue (Klüver-Barrera staining). Slides were examined with the Axioplan 2 microscope (Carl Zeiss; Oberkochen, Germany). For immunofluorescence microscopy, 4% paraformaldehyde-fixed brain specimens were washed with PBS at 4C, immersed in a 10–20% sucrose concentration ascending series in PBS overnight at 4C, and embedded in optimal cutting temperature compound (OCT; Sakura Finetek Torrance, CA) on dry ice. Five-μm-thick frozen sections were cut by a cryostat microtome and washed with PBS. After blocking with 10% normal goat serum for 30 min at room temperature, sections were incubated with a 1 μg/ml solution of each anti-NDRG antibody, a 1:200 dilution of anti-CNPase, a 1:200 dilution of anti-GFAP, and a 1:200 dilution of anti-NeuN overnight at 4C. They were then incubated with a 1:200 dilution of AlexaFluor 488-conjugated anti-rabbit IgG antibody and/or a 1:200 dilution of AlexaFluor 546-conjugated anti-mouse IgG antibody (Invitrogen; Carlsbad, CA) for 1 hr at room temperature. Fluorescence was detected with the Axiovert 200 microscope and photographed with the AxioCam (Carl Zeiss). For negative controls of immunostaining, normal rabbit IgG was used as a primary antibody instead of as a specific antibody.

Results

Raising Specific Antibodies Against the NDRG Family Proteins

We previously raised antibodies against human NDRG1 and NDRG4 (Agarwala et al. 2000; Zhou et al. 2001). Western blotting analysis showed that anti-NDRG1 and anti-NDRG4 specifically reacted with recombinant mouse NDRG1-GFP and NDRG4-GFP, respectively, and that anti-NDRG1 faintly cross-reacted with recombinant mouse NDRG3-GFP (Figure 1). In addition to these antibodies, in the present study we raised antibodies against mouse NDRG2 and NDRG3. They specifically reacted with recombinant mouse NDRG2-GFP and NDRG3-GFP, respectively, without any cross-reactions (Figure 1).

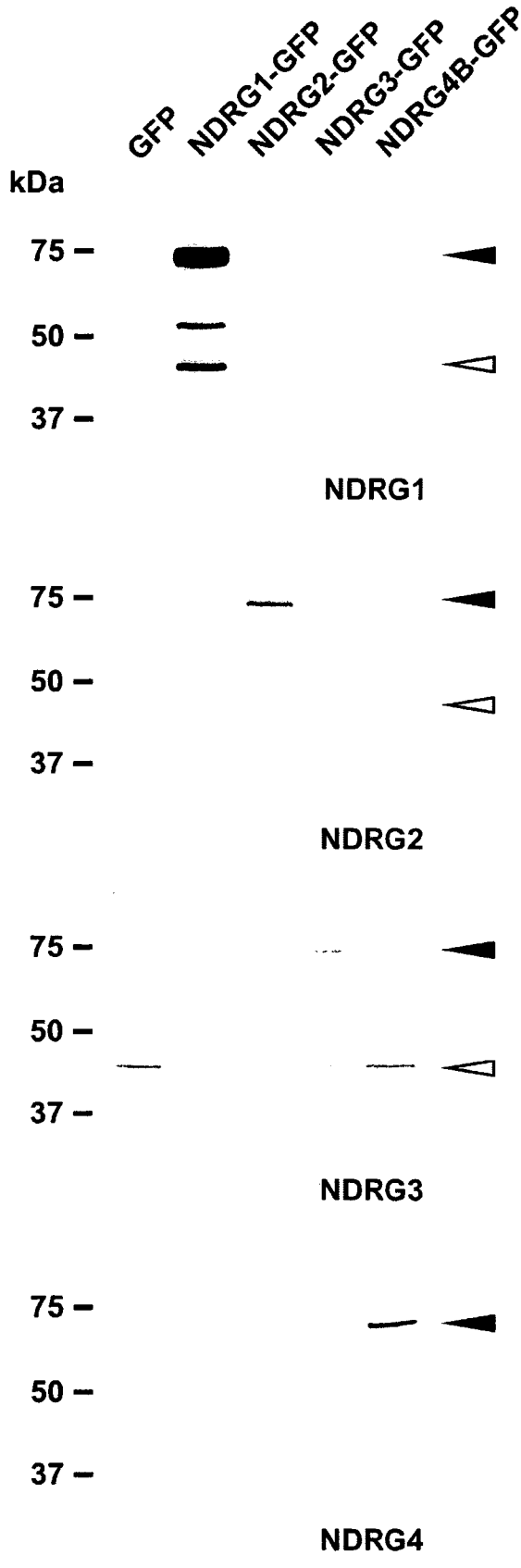

Figure 1 Antibody specificity against NDRG family proteins. Lysates of COS-1 cells transfected with green fluorescent protein (GFP) or mouse NDRG–GFP vectors were analyzed by Western blotting. Each antibody specifically reacted with respective NDRG–GFP fusion proteins (closed arrowheads). Bands indicated by open arrowheads were endogenous NDRG proteins. Each lane contained 5 μg of total protein.

Using these antibodies, we detected all the NDRG family proteins in the brain of wild-type mice aged 4 and 12 weeks (Figure 2). Expression amounts of NDRG2, NDRG3, and NDRG4 proteins were not affected in the brain of *Ndrg1*-deficient mice, suggesting that the loss of NDRG1 did not affect expression levels of the other NDRGs (Figure 2).

Histological Assessment of the Brain of *Ndrg1*-deficient Mice

We previously reported the phenotypes of *Ndrg1*-deficient mice (Okuda et al. 2004). They exhibited muscle weakness caused by peripheral nerve degeneration, but their complicated motor abilities were relatively retained. These phenotypes suggest that CNS can withstand the loss of NDRG1. According to the analysis of conventional histological sections,

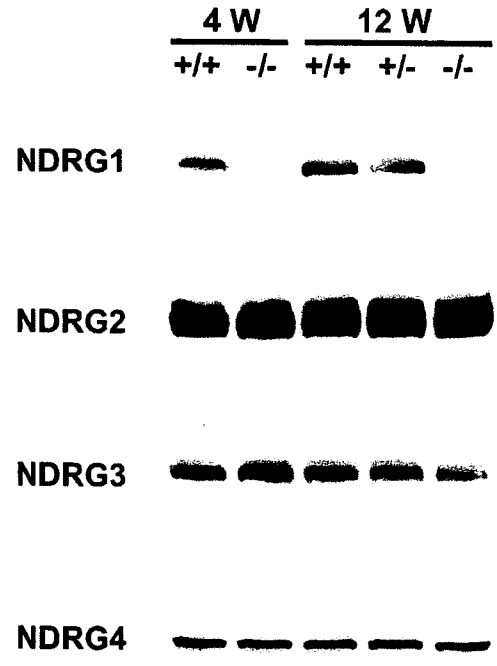

Figure 2 Expression of NDRG family proteins in the mouse brain. Brain lysates were prepared from the wild-type and *Ndrg1*-deficient mice aged 4 or 12 weeks and analyzed by Western blotting. Each lane contained 5 μg of total protein. $^{+/+}$, wild-type mice; $^{-/-}$, homozygous *Ndrg1*-deficient mice; $^{+/-}$, heterozygous *Ndrg1*-deficient mice.

no abnormalities were observed in the brain of *Ndrg1*-deficient mice (Figure 3). Organization of the cerebral cortices and other laminated regions seemed normal (Figures 3A and 3B). The structure of the hippocampus in the *Ndrg1*-deficient mice was not different from the wild-type one (Figures 3C and 3D). Luxol–fast blue staining for the myelin sheaths revealed that myelination was not affected in the brain of *Ndrg1*-deficient mice (Figures 3E and 3F). Immunohistochemical analysis of the wild-type mouse brain using anti-NDRG1 antibody exhibited specific staining in the axon bundles of the corpus callosum, corpus striatum, and fimbria hippocampus (Figure 3G). These NDRG1-staining signals were not detected in the *Ndrg1*-deficient mouse brain (Figure 3H).

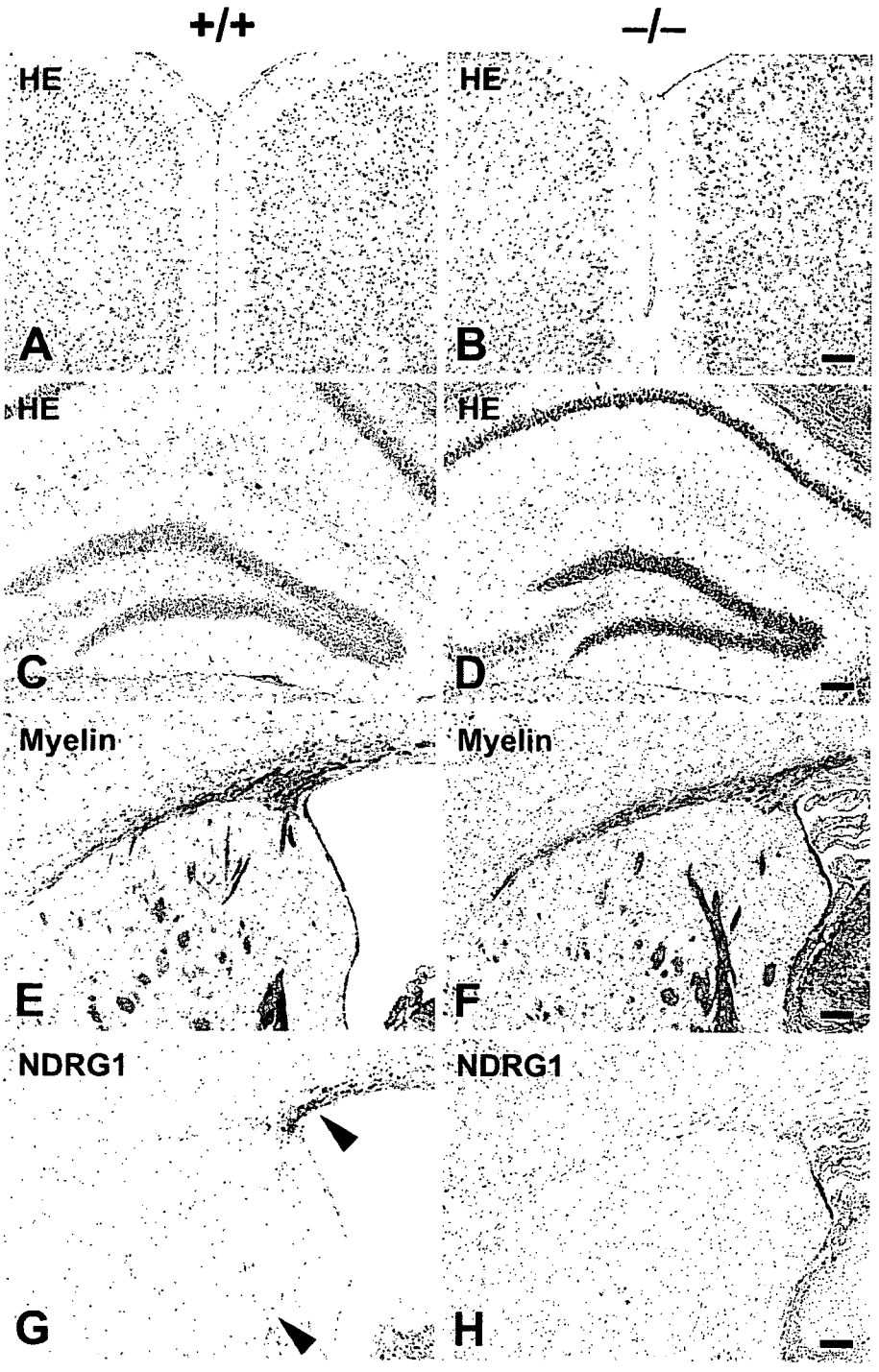

Figure 3 Histological assessment of the brain of adult *Ndrg1*-deficient mice. Transverse sections of cerebral neocortex (**A,B**) and hippocampus (**C,D**) of adult wild-type ($^{+/+}$; **A,C**) and adult *Ndrg1*-deficient ($^{-/-}$; **B,D**) mice were compared. There were no significant differences in the structure of the brain regardless of genotype. Transverse sections of the forebrain at the level of the corpus callosum (**E,F**) and lateral ventricle (**G,H**) of adult wild-type (**E,G**) and adult *Ndrg1*-deficient (**F,H**) mice were compared. Normal myelination was observed in wild-type (**E**) and *Ndrg1*-deficient mice (**F**). NDRG1 was detected in the axon bundles of the corpus callosum and corpus striatum in wild-type mice (arrowheads in **G**). NDRG1 expression was not detected in the *Ndrg1*-deficient mice (**H**). HE, hematoxylin–eosin staining; myelin, luxol–fast blue staining; NDRG1, anti-NDRG1 immunostaining. Bar = 100 μm.

Expression Patterns of NDRGs in the Brain

To investigate the expression characteristics of NDRGs in the brain, we performed immunohistochemical analysis using the antibodies specific for each NDRG. First, NDRG1 was strongly detected in the cytoplasm of oligodendrocytes in the cerebrum (Figure 4A). Specific expression of NDRG1 in the oligodendrocytes was confirmed by double staining for NDRG1 and CNPase. CNPase is a marker for oligodendrocytes (Figures 4C–4E). Although the cytoplasm was a principal site of NDRG1 localization, a fibrous staining pattern was also detected, suggesting that NDRG1 was partially localized in the processes of oligodendrocytes. In addition to the oligodendrocyte localization, weaker staining of NDRG1 was detected in Purkinje cells of the cerebellum (Figure 4B). NDRG1 was also strongly expressed in ependymal cells in the cerebrum (data not shown).

NDRG2 was strongly detected in the astrocytes of the cerebrum (Figure 5A), which was confirmed by double staining for NDRG2 and GFAP (Figures 5C–5E). GFAP is a commonly used marker for astrocytes. In the cerebellum, NDRG2 was also detected in Bergmann glial cells (Figure 5B). In both the cerebrum and cerebellum, NDRG2 was moderately expressed in most cells except neurons in the cerebral cortex and in Purkinje cells in the cerebellum (Figures 5A and 5B). Double staining for NDRG2 and NeuN indicated that NeuN-positive cells were NDRG2 negative in the cerebrum (Figures 5F–5H). NeuN is a marker for neurons. NDRG2 was less expressed in oligodendrocytes (data not shown). In the presence of immunogen peptides, anti-NDRG2 antibody did not give any signals (data not shown).

In contrast to the cytoplasmic localization of NDRG1 and NDRG2, expression of NDRG3 was observed in the nuclei of most cells in the cerebrum (Figure 6A). Nuclear localization of NDRG3 was also observed in other tissues (data not shown). Expression of NDRG3 was relatively strong in the neurons because most of the strong NDRG3-positive cells were NeuN-positive neurons (Figures 6C–6E). Significant expression of NDRG3 was also seen in the nuclei of Purkinje cells in the cerebellum, with less expression in the granule cells (Figure 6B). In the presence of immunogen peptides, anti-NDRG3 antibody did not give any signals (data not shown).

Expression of NDRG4 was detected in most brain cells, especially in the neurons of the cerebrum (Figure 7A, arrowhead) and Purkinje cells of the cerebellum (Figure 7B, open arrowhead). NDRG4-positive cells corresponded to cells expressing a neuron marker NeuN (Figures 7C–7E). NDRG4 was dominantly localized in the cytoplasm of these cells. Cytoplasmic localization of NDRG4 in Purkinje cells (Figure 7B) was similar to that of NDRG1 (Figure 4B). NDRG4 was less expressed in granule cells (Figure 7B) like NDRG1 (Figure 4B).

Discussion

Although NDRG1 is essential for structural and functional maintenance of myelin sheaths in the peripheral nervous system (PNS) (Okuda et al. 2004), the morphology of the brain was not affected by the loss of NDRG1 (Figure 3). To understand the tissue- and cell-specific roles of NDRGs, the localization of each NDRG should be clarified in detail. In the present study we developed specific antibodies and examined

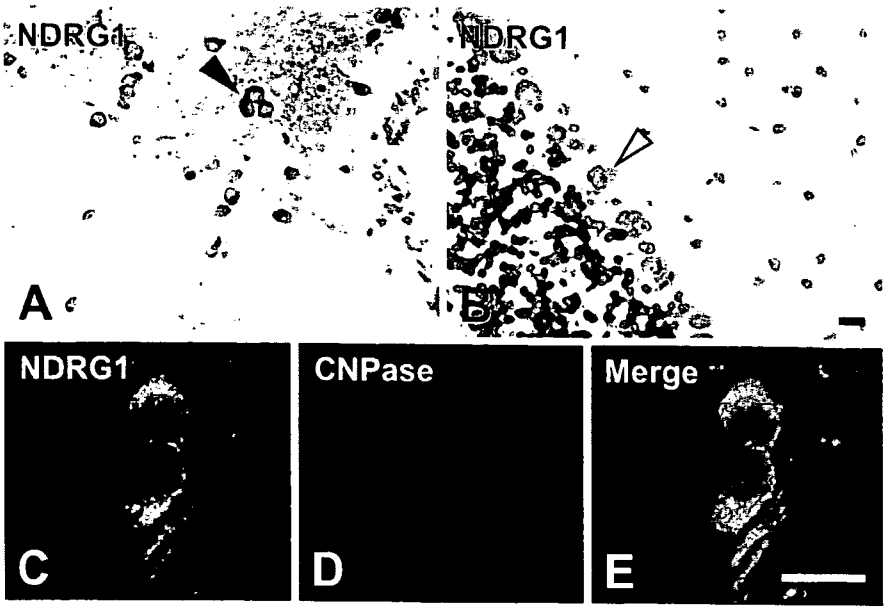

Figure 4 Localization of NDRG1 in the brain. NDRG1 was detected in the cytoplasm of the oligodendrocyte in the cerebrum (arrowhead in **A**) and in Purkinje cells in the cerebellum (open arrowhead in **B**). Expression of NDRG1 (**C**) was colocalized with an oligodendrocyte-specific marker CNPase (**D**). Merged image is shown in **E**. Bar = 10 μm.

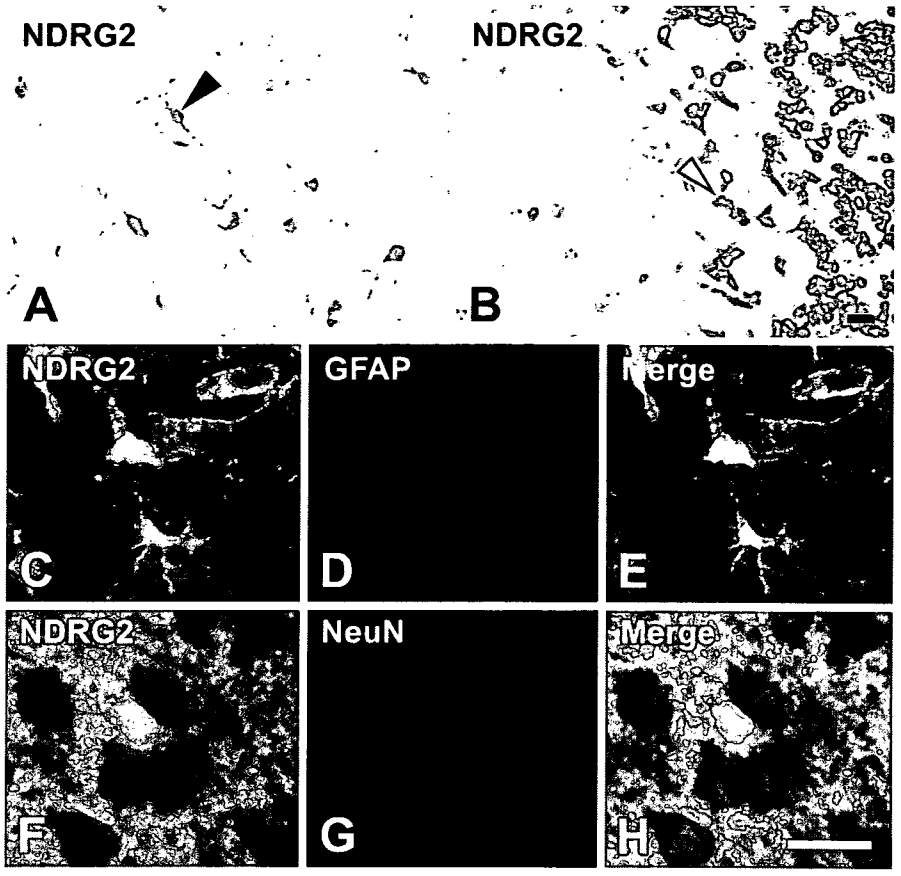

Figure 5 Localization of NDRG2 in the brain. NDRG2 was detected in the astrocytes in the cerebrum (arrowhead in A) and in Bergmann glial cells in the cerebellum (open arrowhead in B). Expression of NDRG2 (C,F) was colocalized with an astrocyte-specific marker GFAP (D), but not with a neuron marker NeuN (G). Merged images are shown in E and H, respectively. Bar = 10 μm.

the expression patterns of NDRGs in the mouse CNS. The expression patterns of each NDRG are summarized in Table 1.

Antibody specificity was examined by Western blotting analysis using recombinant NDRG–GFP fusion proteins. Each antibody specifically reacted with the corresponding protein, although the anti-NDRG1 antibody exhibited a weak cross-reaction to NDRG3 (Figure 1). This may be caused by a relatively high identity of NDRG3 to NDRG1 in amino acid sequence compared

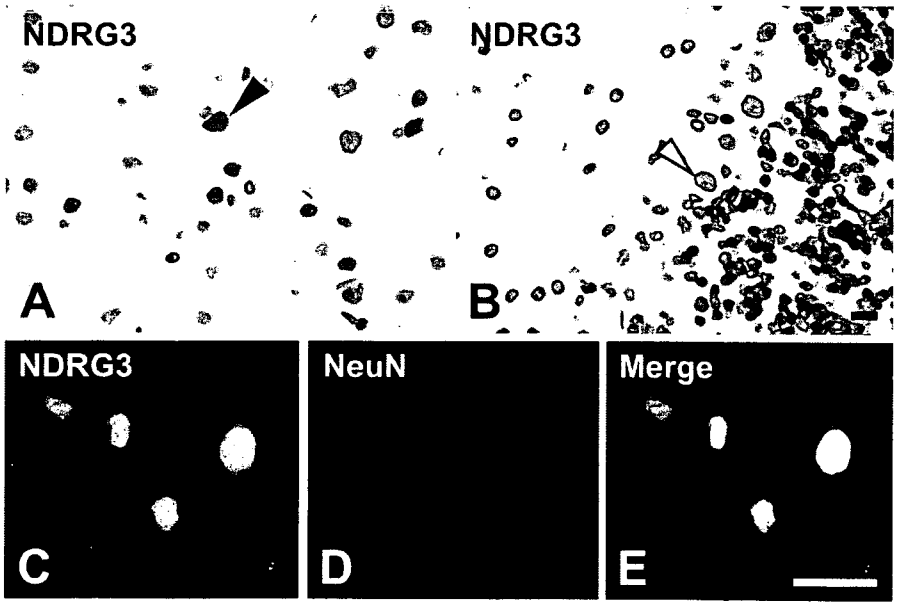

Figure 6 Localization of NDRG3 in the brain. NDRG3 was detected in the nucleus of most cells in the cerebrum, but especially strongly in the neurons (arrowhead in A) and nucleus of Purkinje cells in the cerebellum (open arrowhead in B). Expression of NDRG3 (C) was colocalized with a neuron marker NeuN (D). Merged images are shown in E. Bar = 10 μm.

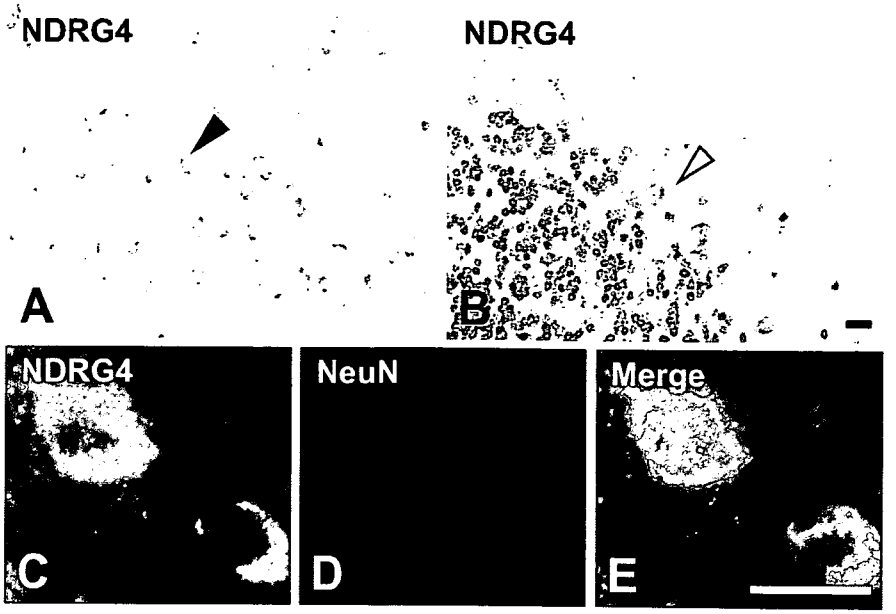

Figure 7 Localization of NDRG4 in the brain. NDRG4 was detected in most cells in the cerebrum, but especially strongly in the neurons (arrowhead in A) and Purkinje cells in the cerebellum (open arrowhead in B). Strong expression of NDRG4 (C) was colocalized with a neuron marker NeuN (D). Merged images are shown in E. Bar = 10 μm.

with NDRG2 and NDRG4. Immunohistochemical analysis, however, could fortunately discriminate NDRG1 from NDRG3: anti-NDRG1 showed a cytoplasmic staining pattern in particular cells, whereas anti-NDRG3 reacted with the nuclei in most cells of the brain.

We demonstrated here that NDRG1 was mainly localized in the oligodendrocytes (Figure 4). Another group (Wakisaka et al. 2003), however, has reported immunohistochemical data inconsistent with the present study. That report demonstrated that the localization of NDRG1 is changed from hippocampal neurons to astrocytes during postnatal development in the rat brain. Although the inconsistency may be caused by the difference in animal species or developmental process, the possibility of unexpected cross-reactions of their antibody to other NDRGs (probably NDRG2) cannot be ruled out. In fact, our observation of NDRG1 localization in oligodendrocytes is consistent with that of another report (Berger et al. 2004).

The oligodendrocyte is a glial cell engaged in the formation of myelin sheaths in the CNS, whereas the Schwann cell expressing NDRG1 plays an analogous role in the PNS. NDRG1, therefore, may contribute to cellular processes in the development or maintenance of myelin sheaths. Although the loss of NDRG1 in Schwann cells led to demyelination in the sciatic nerves (Okuda et al. 2004), the loss in oligodendrocytes had no effect in the brain (Figure 3). These observations suggested that other NDRGs may compensate for the NDRG1 deficiency in oligodendrocytes but cannot do so in Schwann cells. In fact, all NDRGs except NDRG1 were less expressed in the sciatic nerve than in the brain (Okuda et al. 2004).

NDRG2 was localized to the astrocytes in the cerebrum and to Bergmann glial cells in the cerebellum (Figure 5). NDRG3 was expressed in most cells in the cerebrum and cerebellum, and the subcellular localization of NDRG3 was restricted in the nucleus (Figure 6). These marked differences from NDRG1 in the cellular and subcellular localization suggested that NDRG2 and NDRG3 may not have a redundant function of NDRG1. In fact, NDRG2 and NDRG3 were unable to compensate for the NDRG1 deficiency in sciatic nerves despite their expression in the tissue (Okuda et al. 2004).

In contrast to NDRG2 and NDRG3, NDRG4 may be a likely candidate of compensators for the NDRG1 deficiency in the brain. NDRG4 was abundantly expressed in the brain, especially in the neurons and Purkinje cells (Figure 7), the latter of which were also rich in NDRG1. NDRG1 was originally identified as a gene upregulated with homocysteine treatment (Kokame et al. 1996), and expression of NDRG4 is also induced by homocysteine (Nishimoto et al. 2003). These similarities between NDRG1 and NDRG4 may signify their functional similarity. Failure in compensation for the loss of NDRG1 in the *Ndrg1*-deficient PNS can be explained by the fact that there is little expression of NDRG4 in the sciatic nerves (Okuda et al.

Table 1 Summary of major expression cells of NDRG family proteins in the brain

	NDRG1	NDRG2	NDRG3	NDRG4
Cerebrum	Oligodendrocytes Ependymal cells	Astrocytes	Most cells (nucleus)	Most cells
Cerebellum	Purkinje cells	Bergmann glia	Purkinje cells (nucleus) Most cells (nucleus)	Purkinje cells

2004). Further analysis, however, will be needed to clarify the functional specificity and redundancy of NDRGs in the CNS and also in other physiological systems. Developing and analyzing knockout mice for NDRG2, NDRG3, and NDRG4 would be the most effective approach.

Acknowledgments

This work was supported in part by Grants-in-Aid from the Ministry of Health, Labor, and Welfare of Japan; the Ministry of Education, Culture, Sports, Science, and Technology of Japan; and the Program for the Promotion of Fundamental Studies in Health Sciences of the National Institute of Biomedical Innovation (NIBIO).

Literature Cited

Agarwala KL, Kokame K, Kato H, Miyata T (2000) Phosphorylation of RTP, an ER stress-responsive cytoplasmic protein. Biochem Biophys Res Commun 272:641–647

Bandyopadhyay S, Pai SK, Gross SC, Hirota S, Hosobe S, Miura K, Saito K, et al. (2003) The Drg-1 gene suppresses tumor metastasis in prostate cancer. Cancer Res 63:1731–1736

Berger P, Sirkowski EE, Scherer SS, Suter U (2004) Expression analysis of the N-Myc downstream-regulated gene 1 indicates that myelinating Schwann cells are the primary disease target in hereditary motor and sensory neuropathy-Lom. Neurobiol Dis 17:290–299

Guan RJ, Ford HL, Fu Y, Li Y, Shaw LM, Pardee AB (2000) Drg-1 as a differentiation-related, putative metastatic suppressor gene in human colon cancer. Cancer Res 60:749–755

Kalaydjieva L, Gresham D, Gooding R, Heather L, Baas F, de Jonge R, Blechschmidt K, et al. (2000) N-myc downstream-regulated gene 1 is mutated in hereditary motor and sensory neuropathy-Lom. Am J Hum Genet 67:47–58

Kalaydjieva L, Hallmayer J, Chandler D, Savov A, Nikolova A, Angelicheva D, King RH, et al. (1996) Gene mapping in Gypsies identifies a novel demyelinating neuropathy on chromosome 8q24. Nat Genet 14:214–217

Kokame K, Kato H, Miyata T (1996) Homocysteine-respondent genes in vascular endothelial cells identified by differential display analysis. GRP78/BiP and novel genes. J Biol Chem 271: 29659–29665

Kovacevic Z, Richardson DR (2006) The metastasis suppressor, Ndrg-1: a new ally in the fight against cancer. Carcinogenesis 27: 2355–2366

Kurdistani SK, Arizti P, Reimer CL, Sugrue MM, Aaronson SA, Lee SW (1998) Inhibition of tumor cell growth by RTP/rit42 and its responsiveness to p53 and DNA damage. Cancer Res 58: 4439–4444

Nishimoto S, Tawara J, Toyoda H, Kitamura K, Komurasaki T (2003) A novel homocysteine-responsive gene, smap8, modulates mitogenesis in rat vascular smooth muscle cells. Eur J Biochem 270:2521–2531

Okuda T, Higashi Y, Kokame K, Tanaka C, Kondoh H, Miyata T (2004) Ndrg1-deficient mice exhibit a progressive demyelinating disorder of peripheral nerves. Mol Cell Biol 24:3949–3956

Okuda T, Kondoh H (1999) Identification of new genes Ndr2 and Ndr3 which are related to Ndr1/RTP/Drg1 but show distinct tissue specificity and response to N-myc. Biochem Biophys Res Commun 266:208–215

Piquemal D, Joulia D, Balaguer P, Basset A, Marti J, Commes T (1999) Differential expression of the RTP/Drg1/Ndr1 gene product in proliferating and growth arrested cells. Biochim Biophys Acta 1450:364–373

Qu X, Zhai Y, Wei H, Zhang C, Xing G, Yu Y, He F (2002) Characterization and expression of three novel differentiation-related genes belong to the human NDRG gene family. Mol Cell Biochem 229:35–44

Shimono A, Okuda T, Kondoh H (1999) N-myc-dependent repression of *Ndr1*, a gene identified by direct subtraction of whole mouse embryo cDNAs between wild type and *N-myc* mutant. Mech Dev 83:39–52

Stein S, Thomas EK, Herzog B, Westfall MD, Rocheleau JV, Jackson RS 2nd, Wang M, et al. (2004) NDRG1 is necessary for p53-dependent apoptosis. J Biol Chem 279:48930–48940

van Belzen N, Dinjens WN, Diesveld MP, Groen NA, van der Made AC, Nozawa Y, Vlietstra R, et al. (1997) A novel gene which is up-regulated during colon epithelial cell differentiation and down-regulated in colorectal neoplasms. Lab Invest 77:85–92

Wakisaka Y, Furuta A, Masuda K, Morikawa W, Kuwano M, Iwaki T (2003) Cellular distribution of NDRG1 protein in the rat kidney and brain during normal postnatal development. J Histochem Cytochem 51:1515–1525

Xu B, Lin L, Rote NS (1999) Identification of a stress-induced protein during human trophoblast differentiation by differential display analysis. Biol Reprod 61:681–686

Zhou D, Salnikow K, Costa M (1998) *Cap43*, a novel gene specifically induced by Ni^{2+} compounds. Cancer Res 58:2182–2189

Zhou RH, Kokame K, Tsukamoto Y, Yutani C, Kato H, Miyata T (2001) Characterization of the human NDRG gene family: a newly identified member, NDRG4, is specifically expressed in brain and heart. Genomics 73:86–97

Journal of Thrombosis and Haemostasis, 5: 1–3 DOI: 10.1111/j.1538-7836.2007.02828.x

LETTERS TO THE EDITOR

Inherited and *de novo* mutations of *ADAMTS13* in a patient with Upshaw-Schulman syndrome

K. KOKAME, * Y. AOYAMA, † M. MATSUMOTO, ‡ Y. FUJIMURA‡ and T. MIYATA*

**National Cardiovascular Center Research Institute, Suita, Osaka; †Department of Hematology, Seichokai Fuchu Hospital, Izumi, Osaka; and ‡Department of Blood Transfusion Medicine, Nara Medical University, Kashihara, Nara, Japan*

To cite this article: Kokame K, Aoyama Y, Matsumoto M, Fujimura Y, Miyata T. Inherited and *de novo* mutations of *ADAMTS13* in a patient with Upshaw-Schulman syndrome. *J Thromb Haemost* 2007; DOI: 10.1111/j.1538-7836.2007.02828.x.

Upshaw-Schulman syndrome (USS) is a congenital thrombotic and hemorrhagic diathesis characterized by a deficient activity of plasma von Willebrand factor (VWF)-cleaving protease, *ADAMTS13* [1–8]. Some patients with USS develop severe jaundice soon after birth as their first symptom, and some are almost asymptomatic during childhood to adolescence, unless they have precipitating factors such as infection or pregnancy. The pathological condition of USS belongs to thrombotic thrombocytopenic purpura (TTP), which is characterized by thrombocytopenia, hemolytic anemia and microvascular thrombosis. USS, therefore, is also called congenital TTP. Most cases of TTP result from acquired deficient activity of ADAMTS13 caused by the advent of autoantibodies that inhibit the ADAMTS13 activity. In contrast, patients with USS do not carry such inhibitory antibodies in their plasma, and suffer from USS because of the compound heterozygous or homozygous mutations of *ADAMTS13*. More than 80 mutations of the *ADAMTS13* gene have been identified in patients with USS. Here, we report a first case with *de novo* mutations of *ADAMTS13*.

Patient *P* (II-2 in Fig. 1A) is the second child of unrelated Japanese parents (I-1 and I-2). The first child (II-1) was spontaneously aborted from an unknown cause at 6 weeks of pregnancy, while the fourth child (II-4) was aborted by umbilical coiling at 22 weeks. The parents and the third child (II-3) are apparently healthy. The patient showed moderate hyperbilirubinemia soon after birth and received phototherapy without exchange blood transfusion. On the occasion of catching cold at 3 years of age, he developed thrombocytopenia, microangiopathic hemolytic anemia, and renal insufficiency. He was diagnosed as having TTP and treated with fresh frozen plasma (FFP) infusions. Thereafter, he repeated these episodes several times a year, and each time he soon recovered with FFP infusions. At 21 years of age, he developed a hallmark of TTP, consisting of thrombocytopenia, microangiopathic hemolytic anemia, neurological dysfunction, renal failure and fever. He started taking prophylactic infusions of FFP (4–8 ml kg^{-1} body weight) every 2 weeks.

The plasma ADAMTS13 activities of the family members, measured by the method based on VWF-multimer analysis [1,9], are shown under each symbol in Fig. 1A. The ADAMTS13 activity of the patient was less than 3% of that of the control, which was confirmed by measuring his plasma collected after an interval of more than 1 month. The values were consistent with the data obtained by two other methods, a fluorogenic assay [10] and a chromogenic assay [11] (data not shown). As the assay of the ADAMTS13-activity inhibitors [1] showed no detectable inhibitors in the patient plasma (data not shown), the etiology of his TTP symptoms was considered a genetic deficiency of ADAMTS13, that is, USS. To clarify the underlying cause of the TTP crisis, we analyzed the nucleotide sequences of the family's *ADAMTS13* genes.

DNA experiments were carried out with the permission of the ethics committees of the National Cardiovascular Center after obtaining informed consent from the study subjects. The nucleotide sequences of all 29 exons of *ADAMTS13*, including the intron-exon boundaries, were determined by direct sequencing of polymerase chain reaction (PCR) products as described previously [12,13].

The patient was heterozygous for five nucleotide mutations, c.964T > G, c.968C > G, c.969C > A, c.970T > C and c.2723G > A. Of them, c.2723G > A was also detected in the father. The mother and sister were heterozygous for c.2708C > T, which was not found in the patient or his father (Fig. 1B).

The c.2723G > A mutation on exon 21 causing C908Y, heterozygously found in the patient and father, was previously reported by us as a causative mutation in another USS family [14]. This mutation causes the impaired secretion of ADAMTS13 [14]. The moderately decreased ADAMTS13 activity of the father in the present case could be explained by this single mutation. The c.2708C > T mutation on exon 21 causing S903L was heterozygously found in the mother and sister,

Correspondence: Koichi Kokame, National Cardiovascular Center Research Institute, 5-7-1 Fujishirodai, Suita, Osaka 565-8565, Japan. Tel.: +81 6 6833 5012; fax: +81 6 6835 1176; e-mail: kame@ri.ncvc.go.jp

Received 29 October 2007, accepted 29 October 2007

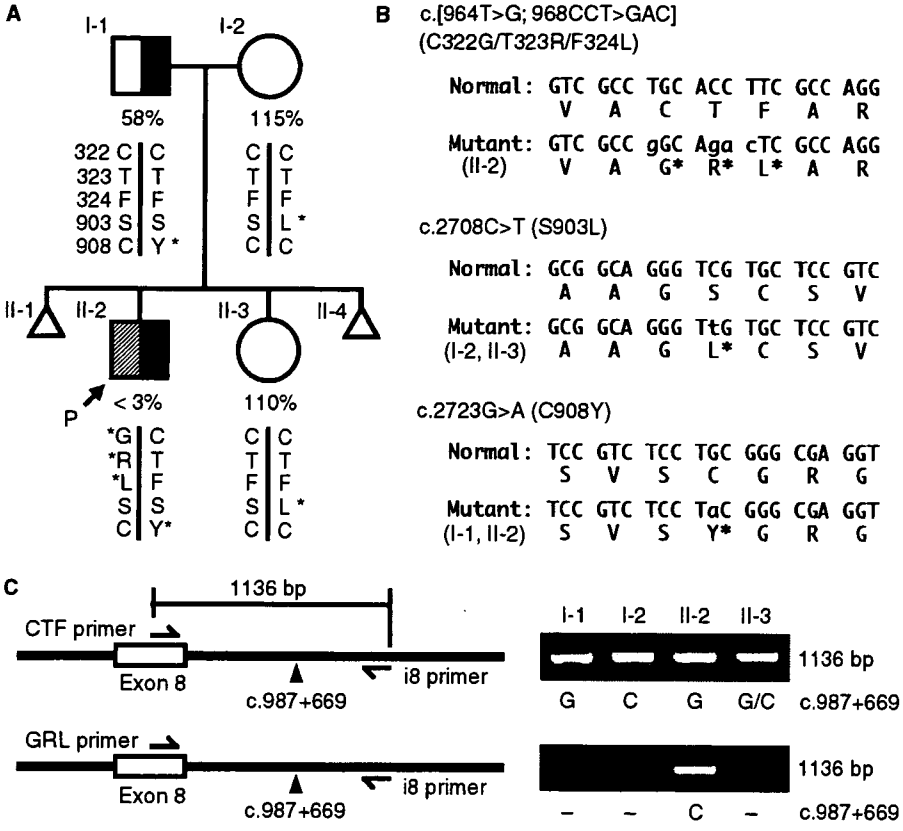

Fig. 1. *ADAMTS13* mutations in the USS patient *P* family. (A) Pedigree of the patient family. Plasma ADAMTS13 activities are shown under each symbol. The haplotype patterns of the five amino-acid residues deduced from each *ADAMTS13* gene are indicated under the ADAMTS13 activities. The arrow indicates the proband. (B) Missense mutations of *ADAMTS13* identified in this family. S903L is a common polymorphism. Asterisks indicate the mutated amino-acid residues. (C) PCR analysis of normal and mutant alleles. The 1,136-bp region was amplified by PCR using either the normal allele-specific CTF primer (5′-CCAAGGCTGTCGCCTGCACCT-3′) or the mutant allele-specific GRL primer (5′-CCAAGGCTGTCGCCGGCAGAC-3′) on exon 8 with the common reverse i8 primer (5′-TGAAGCCAGGAGTCCTAGACA-3′) on intron 8. This region contained a single nucleotide G/C polymorphism at the site of c.987 + 669. Subjects I-1 (father) and I-2 (mother) were homozygotes for G and C, respectively. The normal and mutant alleles of II-2 (patient) carried G and C, respectively.

whose plasma ADAMTS13 activities were normal. This suggested that S903L should not affect the ADAMTS13 activity. In fact, the allele frequency of S903L is 6.0% in the Japanese general population (our unpublished data), making it a common polymorphism.

The four mutations on exon 8, c.964T > G, c.968C > G, c.969C > A and c.970T > C, were detected only in the patient, suggesting that they should be *de novo* mutations in the patient's *ADAMTS13*. All the four mutations were excluded as common polymorphisms by the screening of 346 individuals in the Japanese general population. Cloning and sequencing of the genomic PCR products including exon 8 revealed that all the mutations were located on a single allele. Therefore, they could be described as c.[964T > G; 968CCT > GAC], resulting in three contiguous missense changes C322G/T323R/F324L within the disintegrin-like domain of ADAMTS13. The C322G mutation may disrupt a tertiary structure of the protein because of the defect in disulfide bond formation.

To determine the origin of the freshly mutated allele of the patient, a longer region including exon 8 was amplified by PCR using a combination of either the normal allele-specific CTF primer or the mutant allele-specific GRL primer and the common reverse i8 primer (Fig. 1C). The combinatorial use of CTF and i8 primers produced a 1,136-bp fragment from genomic DNAs of all the family members, whereas the use of GRL and i8 primers produced a 1,136-bp fragment only from the patient, as expected. The region contained a single nucleotide G/C polymorphism at the site of c.987 + 669. Sequencing of the fragments suggested that the father and mother were homozygotes for G and C, respectively, and that the sister was heterozygous. The normal and mutant alleles of the patient carried G and C, respectively. These results suggested that the mutant allele of the patient was derived from one of the maternal alleles. Based on all of the data, we concluded that the patient was a compound heterozygote of paternally transmitted C908Y and freshly mutated C322G/T323R/F324L on the maternal allele.

In conclusion, this is the first report of a case of compound heterozygosity of inherited and *de novo ADAMTS13* mutations resulting in USS.